Supporting Information For:

An Imidazole Functionalized Aqua-Stable Metal-Organic Framework for Selective Fluorogenic Detection of Herbicide DNOC and Antibacterial Agent Furaltadone in Various Biological and Environmental Specimens

Subhrajyoti Ghosh,[ϵ] Sk Sakir Hossain,[ϵ] and Shyam Biswas*

Department of Chemistry, Indian Institute of Technology Guwahati, 781039, Assam, India.

[ϵ]*Equal contribution*

*Corresponding author. Tel: 91-3612583309

E-mail address: sbiswas@iitg.ac.in

Materials and Characterization Methods:

All of the chemicals were purchased from commercial suppliers and used directly. The 2-(2-((1H-imidazol-2-yl)methylene)hydrazinyl)terephthalic acid linker (H_2L) was prepared according to the below mentioned procedure. The Attenuated Total Reflectance Infrared (ATR-IR) spectra were recorded using PerkinElmer UATR Two at the ambient condition in the region 400-4000 cm^{-1}. The notations used for characterization of the bands are broad (br), strong (s), very strong (vs), medium (m), weak (w) and shoulder (sh). Fluorescence sensing studies were performed with a HORIBA JOBIN YVON Fluoromax-4 spectrofluorometer. A Bruker Avance III 600 NMR spectrometer was used for recording ^1H and ^{13}C NMR spectra at 125 MHz. Thermogravimetric analysis (TGA) was carried out with a Netzsch STA-409CD thermal analyzer in the temperature range of 30-700 °C in an O_2 atmosphere at the heating rate of 4 °C min^{-1}. PXRD data were collected by using Rigaku Smartlab X-ray diffractometer with Cu-Kα radiation, 40 kV of operating voltage and 125 mA of operating current. N_2 sorption isotherms were recorded by using Quantachrome Quadrasorb evo volumetric gas adsorption equipment at -196 °C. Before the sorption analysis, the degassing of the compound was carried out at 100 °C under a high vacuum for 24 h. Gemini 500 was utilized for Energy Dispersive X-rays spectrometer (EDX) for elemental characterization. FE-SEM images were captured with a Zeiss (SIGMA 300) scanning electron microscope. Pawley refinement was carried out using Materials Studio software.[1]

Preparation MOF (1') Suspension for Fluorescence Experiments:

We chose water as a sensing medium for the fluorometric detection of DNOC and furaltadone with the thermally activated MOF (**1'**). For the sensing of targeted analytes, 4 mg of **1'** was suspended in 4 mL of distilled water. Subsequently, the prepared suspension was left undisturbed at room temperature overnight to ensure its stability. For the fluorescence experiment, 300 µL of the aforementioned stable suspension was carefully transferred into a quartz container, containing 3 mL of distilled water. Fluorescence measurements were then conducted across the wavelength range of 430-650 nm, with excitation wavelength of 361 nm.

Fluorometric Detection of Furaltadone in Blood Serum Sample:

A 10 mL of blood sample was collected and centrifuged at 10,000 rpm for 15 min to obtain blood plasma. The light-yellow blood serum was collected by centrifugation and stored in a Falcon tube at -20 °C. To conduct fluorescence detection experiments, varying concentrations of furaltadone were added to different aliquots of the blood serum sample containing a MOF suspended in HEPES buffer (pH = 7.4).

Fluorometric Detection of Furaltadone in Urine Sample:

A 10 mL urine sample was collected from a healthy individual. Thereafter, the sample was centrifuged at 8000 rpm for 10 min, and the supernatant was used for the experiments. To conduct fluorescence experiments, various amounts of furaltadone were added to the urine samples containing a HEPES buffer suspension of the probe.

Quantum Yield Measurement:

Here, we have utilised the Parker-Rees method to calculate the quantum yield of the prepared MOF, using a 0.5 M H_2SO_4 solution of quinine sulphate as a standard reference.[2] The formula for this calculation is provided as follows:

$$\Phi_s = (A_r F_s n_s^2 / A_s F_r n_r^2)\, \Phi_r \quad\ldots\ldots\ldots\ldots\ldots\ldots\ldots\ldots\ldots\ldots\ldots\ldots\text{(Equation-1)}$$

In this equation, Φ_r represents the quantum yield of the quinine sulphate reference solution, while Φ_s represents the quantum yield of the sample. The values of A_r and A_s correspond to the absorbance of the reference and sample, respectively, whereas F_r and F_s refer to the integrated area of fluorescence intensity for the reference and sample, respectively. The refractive indices of the reference and sample are represented by n_r and n_s, respectively. Table S1 contains the relevant photophysical parameters and quantum yield values.

Table S1. Quantum yield of quinine sulphate, **1'**, and analyte treated **1'**.

Sl. No.	Sample Name	Excitation Wavelength λ_{ex} (nm)	Absorbance (A)	Area of Integrated Fluorescence Intensity (F)	Quantum Yield (Φ)
1	Quinine Sulphate	344	0.097	3.88E7	0.546
2	**1'**	361	0.072	5.78E6	0.107
3	**1'** after treatment with DNOC	361	0.076	2.64E6	0.049
4	**1'** after treatment with FLT	361	0.074	2.10E6	0.038

Synthetic Procedure for 2-(2-((1H-Imidazol-2-yl)Methylene)Hydrazinyl)Terephthalic Acid (H_2L) Linker:

The linker was synthesized in two steps. In first step, we have synthesized the 2-hydrazineylterephthalic acid by following the reported literature.[3] In second step, 196 mg of 2-hydrazineylterephthalic acid (1 mmol) and 96 mg (1 mmol) of imidazole 2-carboxaldehyde were dissolved in 10 mL of anhydrous MeOH. After that, the reaction mixture was refluxed for 24 h under N_2 atmosphere. After the completion of the reaction the reaction mixture was allowed to cool down to room temperature. The solvent was removed through evaporation under reduced pressure. Finally, the obtained yellow colored product was dried in a hot air oven at 80 °C. Yield: 750 mg (2.38 mmol, 91%). ^{1}H NMR (500 MHz, DMSO-d_6): δ = 11.60 (s, 1H), 8.31 (s, 1H), 8.15 (s, 1H), 7.96-7.94 (d, 1H), 7.34-7.32 (d, 1H), 7.19 (d, 2H) ppm. ^{13}C NMR (125 MHz, DMSO-d_6): δ = 169.22, 167.77, 167.31, 167.16, 146.44, 143.09, 141.56, 135.74, 131.58, 123.77, 118.25, 114.44 ppm. HR-MS (m/z): 275.0778 for $(M+H)^+$ ion (M = 274.0702, mass of H_2L linker). In Figures S1-S3, the NMR and mass spectra of the H_2L linker are shown.
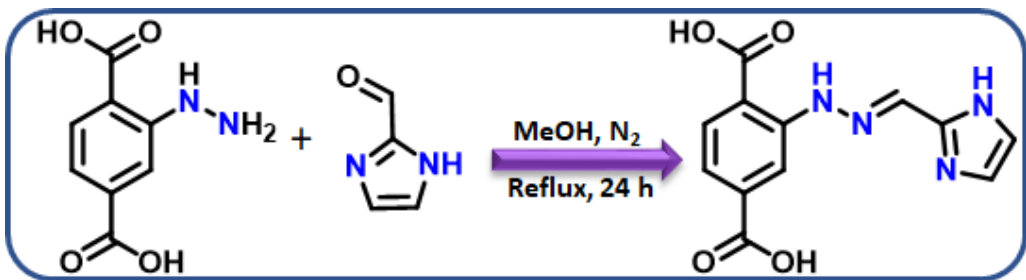
**Scheme S1.** Reaction scheme for the synthesis of H$_2$L linker.
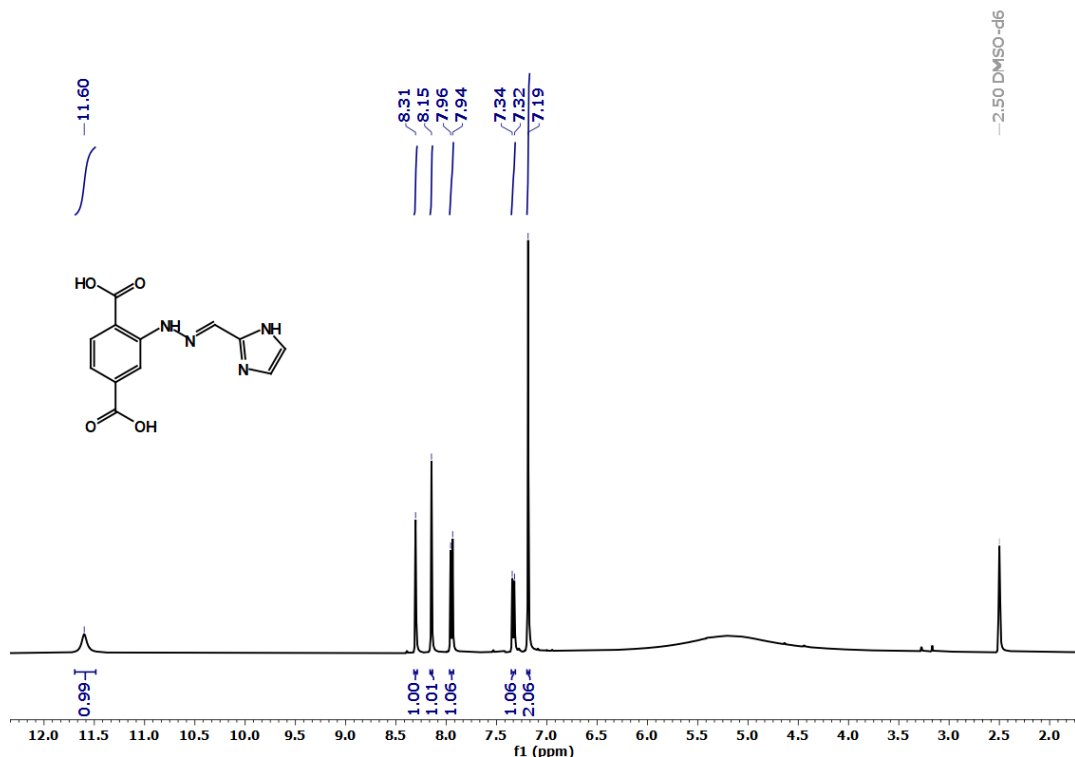
**Figure S1.** ^{1}H NMR spectrum (500 MHz, DMSO-d$_6$) of H$_2$L linker.
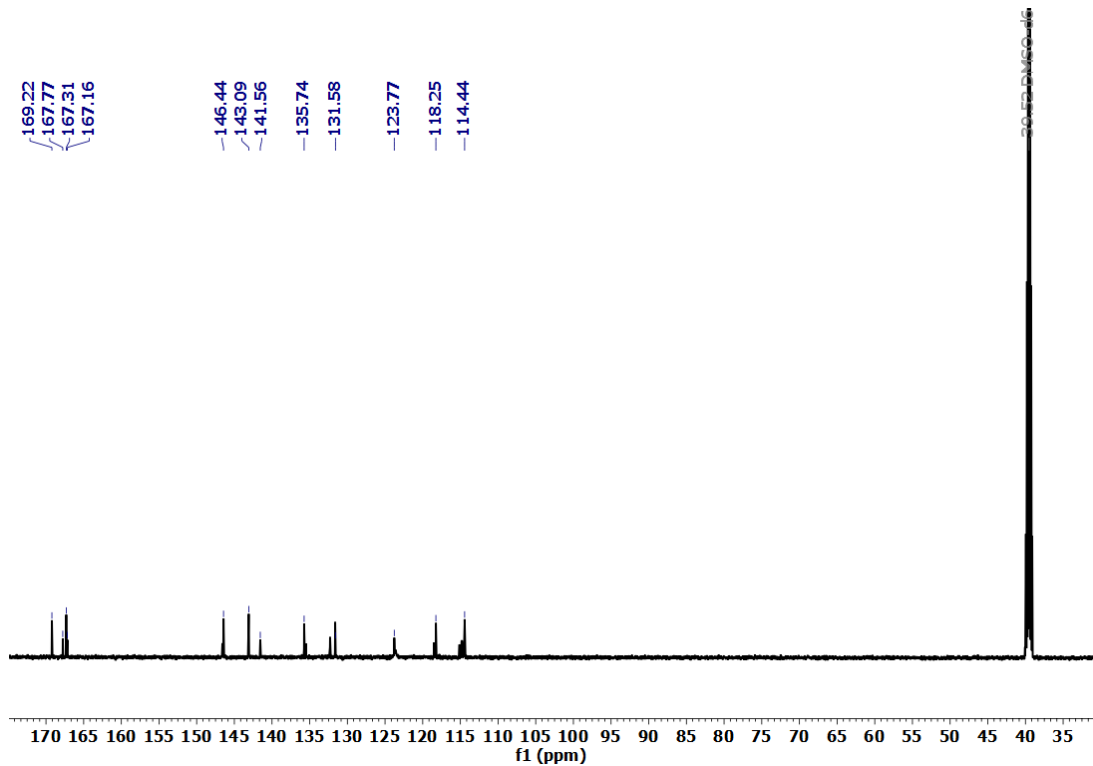
Figure S2. ^{13}C NMR spectrum (125 MHz, DMSO-d$_6$) of H$_2$L linker.
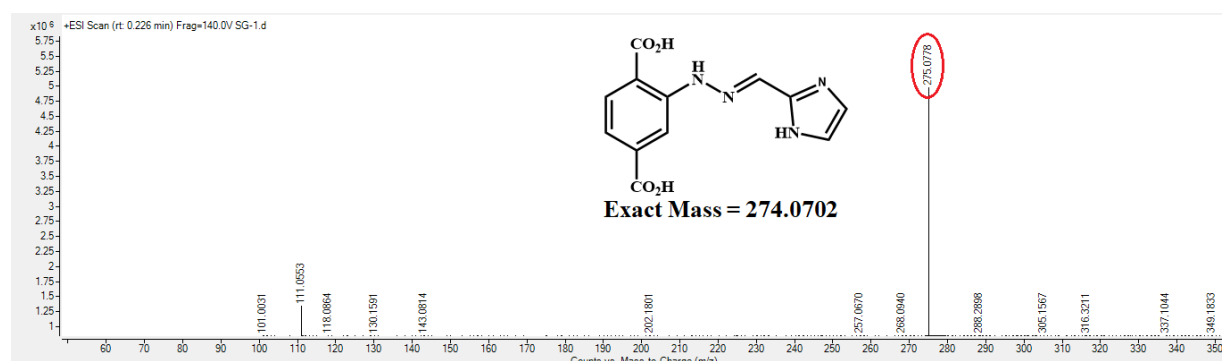

Figure S3. ESI-MS spectrum of H$_2$L linker measured in methanol. The spectrum shows m/z peak at 275.0778, which corresponds to (M+H)$^+$ ion (M = mass of 2-(2-((1H-imidazol-2-yl)methylene)hydrazinyl)terephthalic acid linker).
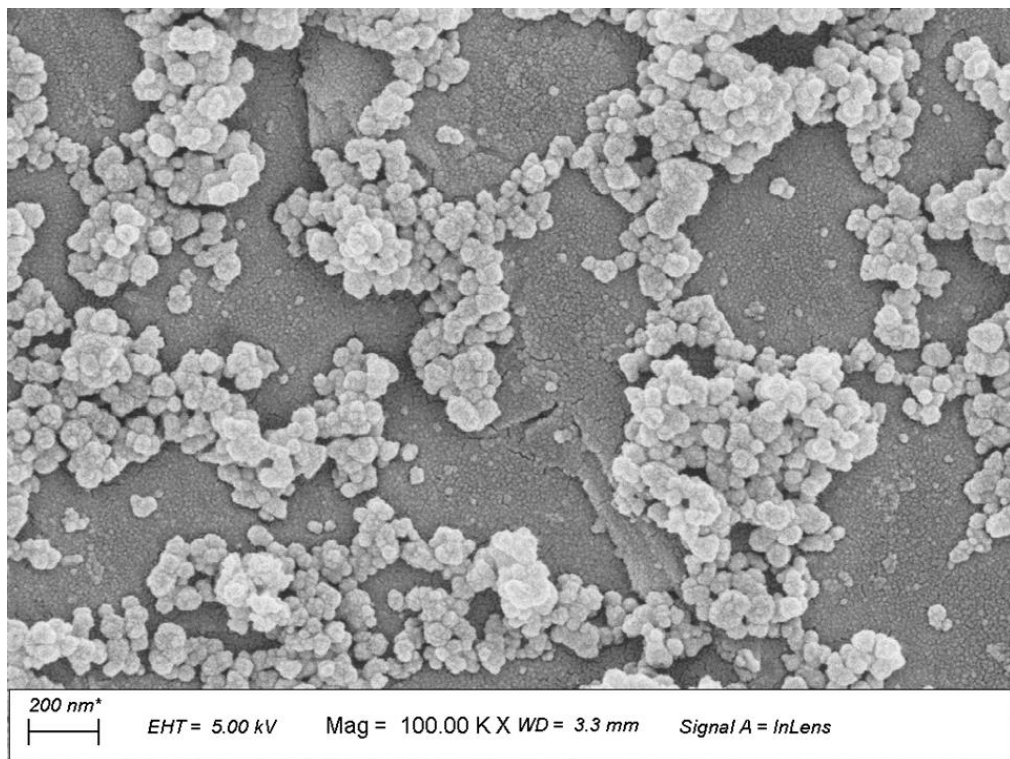
**Figure S4.** FE-SEM image of **1**.
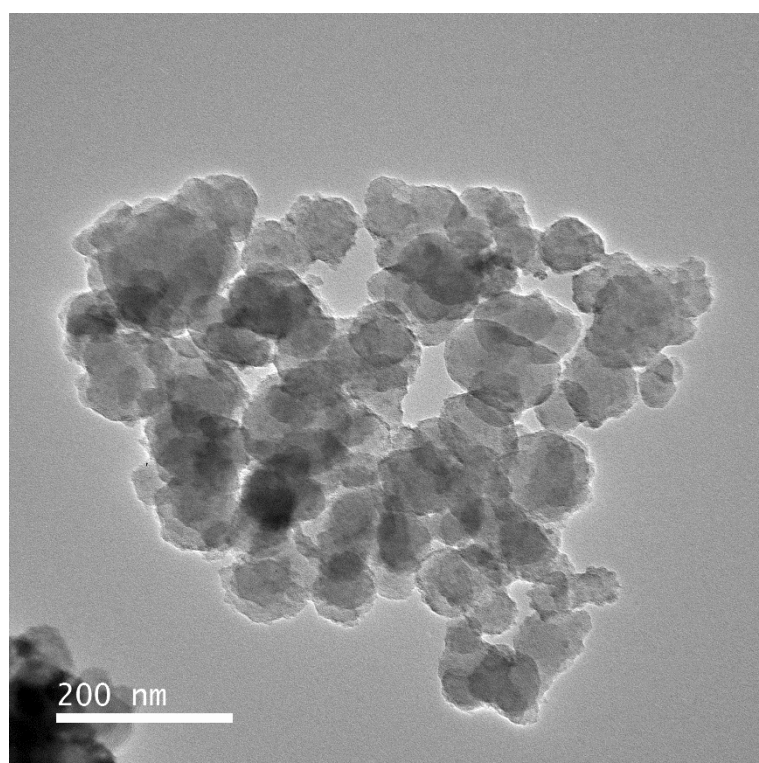
Figure S5. FE-TEM image of **1**.
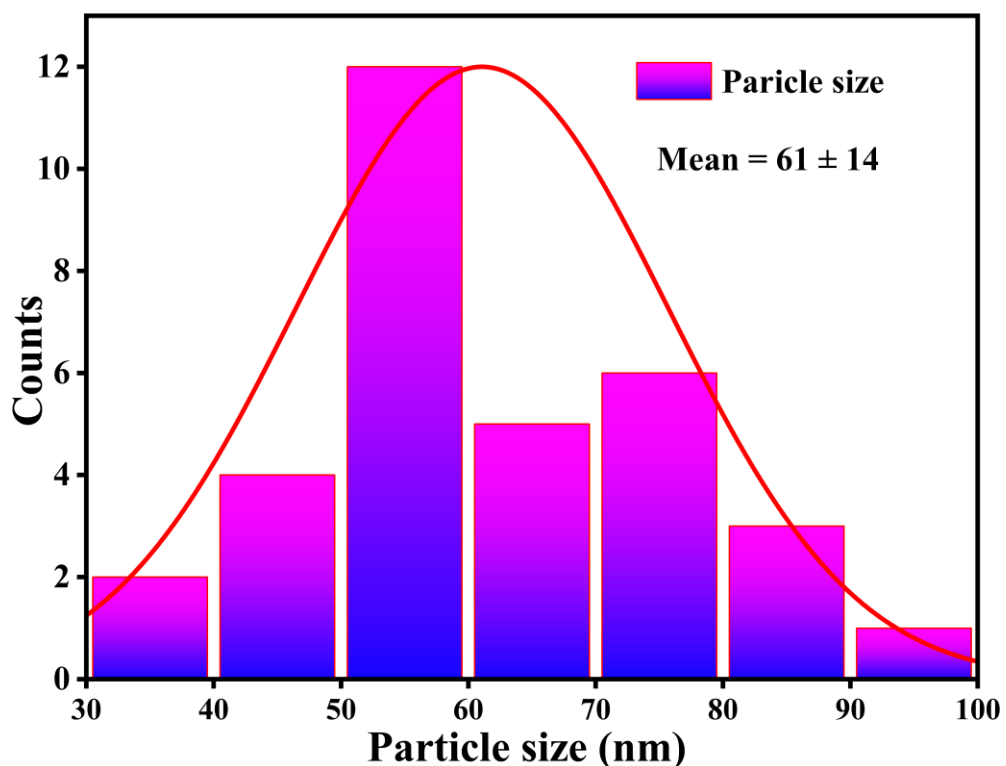
Figure S6. Particle size distribution plot for **1′** (particle sizes were obtained from obtained the TEM images).
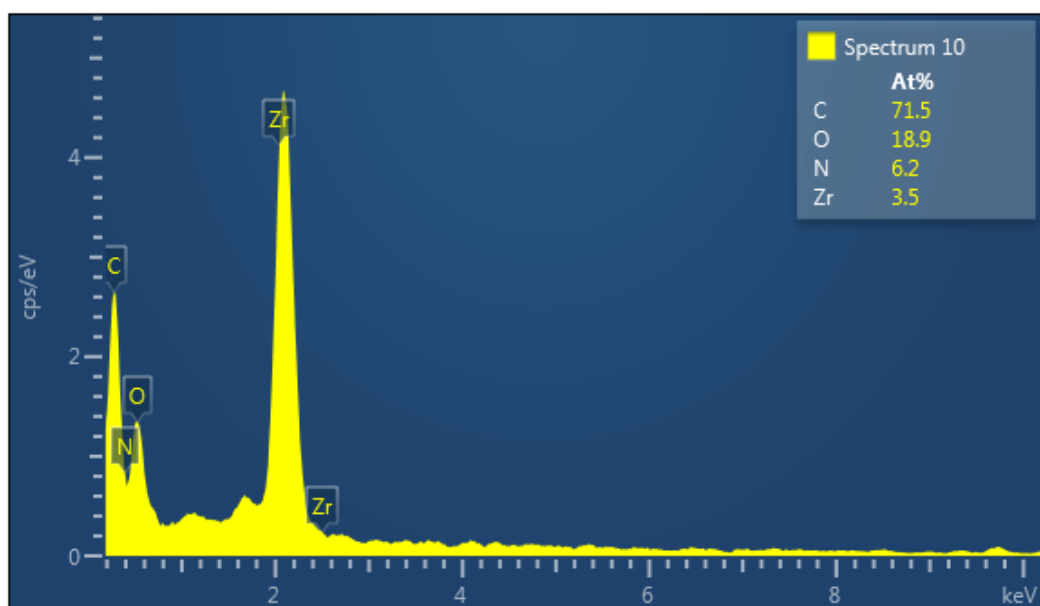

Figure S7. EDX spectrum of **1**.
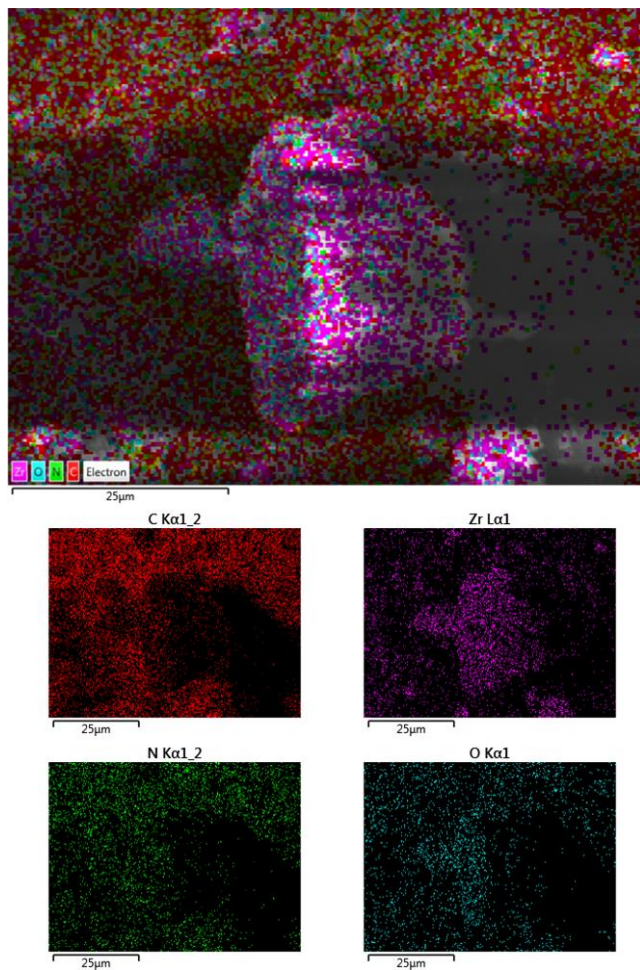
Figure S8. EDX elemental mapping of expected elements present in **1**.
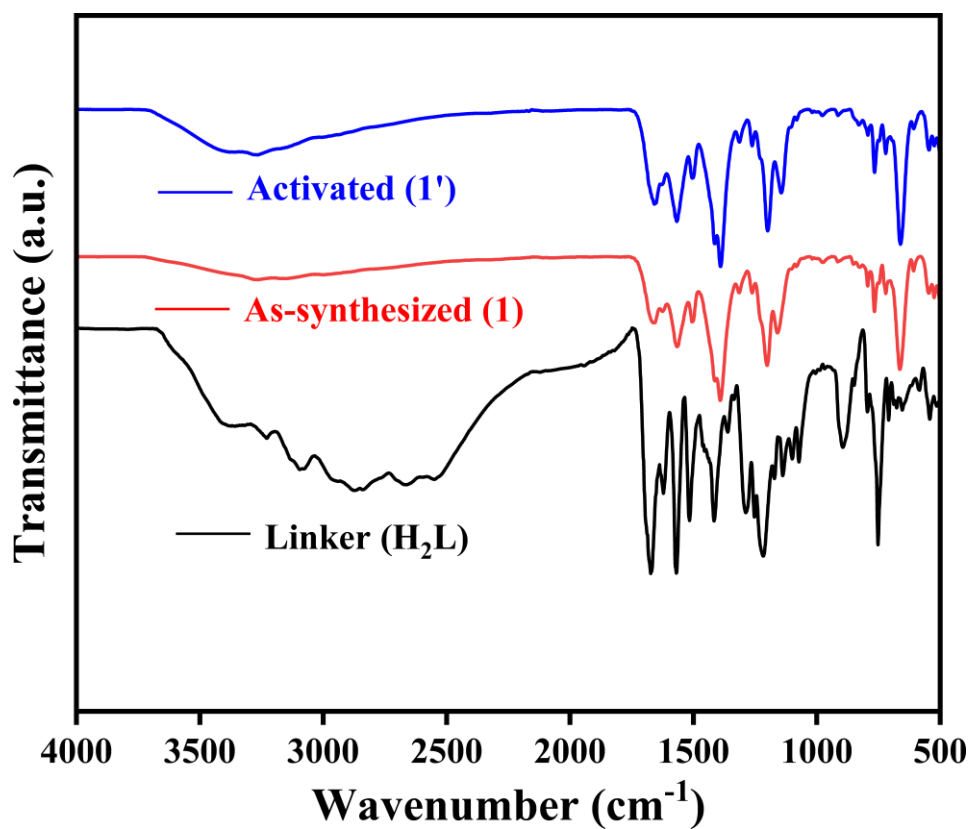
Figure S9. ATR-IR spectra of H_2L linker, **1** and **1'**.
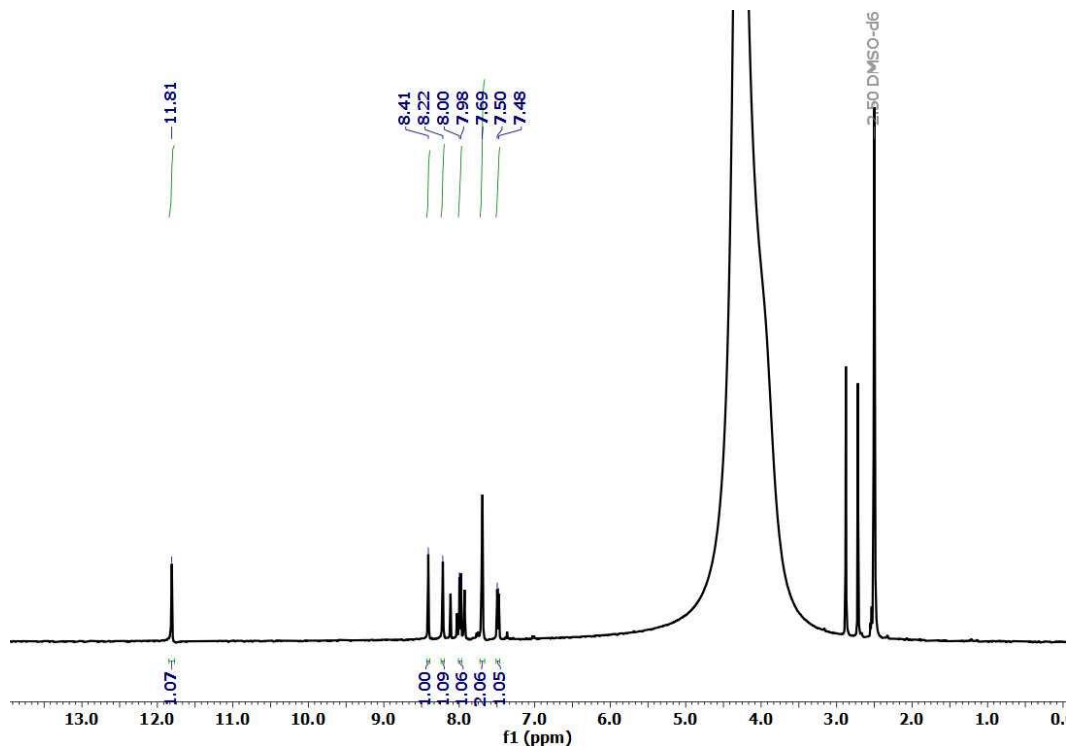
Figure S10. ^{1}H NMR spectrum of digested **1'** (digested using 40 µL of 40% HF in 500 µL of DMSO-d_6).

Table S2. Indexing parameters of UiO-66 and synthesized **1**.

Compound Name	$[Zr_6O_4(OH)_4(C_{12}H_8N_4O_4)_6]\cdot 1.7DMF\cdot 6.2H_2O$ (**1**) (this work)	UiO-66 (reported)[4]
Crystal System	Cubic	Cubic
a = b = c (Å)	20.783 (4)	20.7004(2)
α = β= γ (°)	90	90
V (Å3)	8976.2 (28)	8870.3(2)
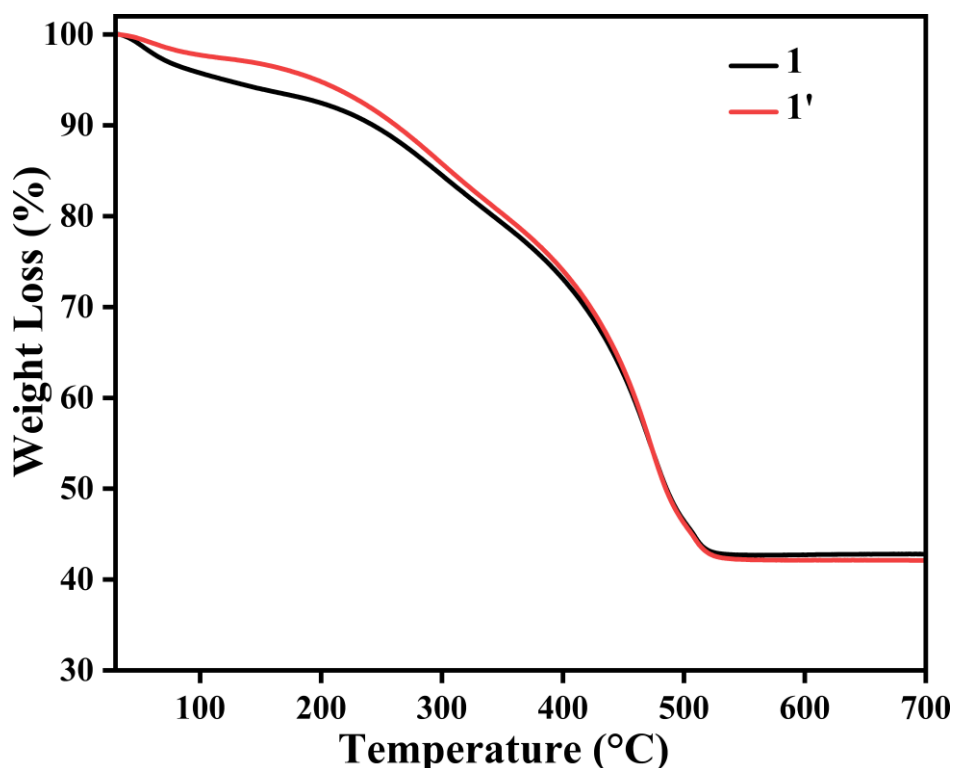
Figure S11. TGA curves of **1** and **1'** recorded under O_2 atmosphere in the temperature range of 30-700 °C with a heating rate of 4 °C/min.
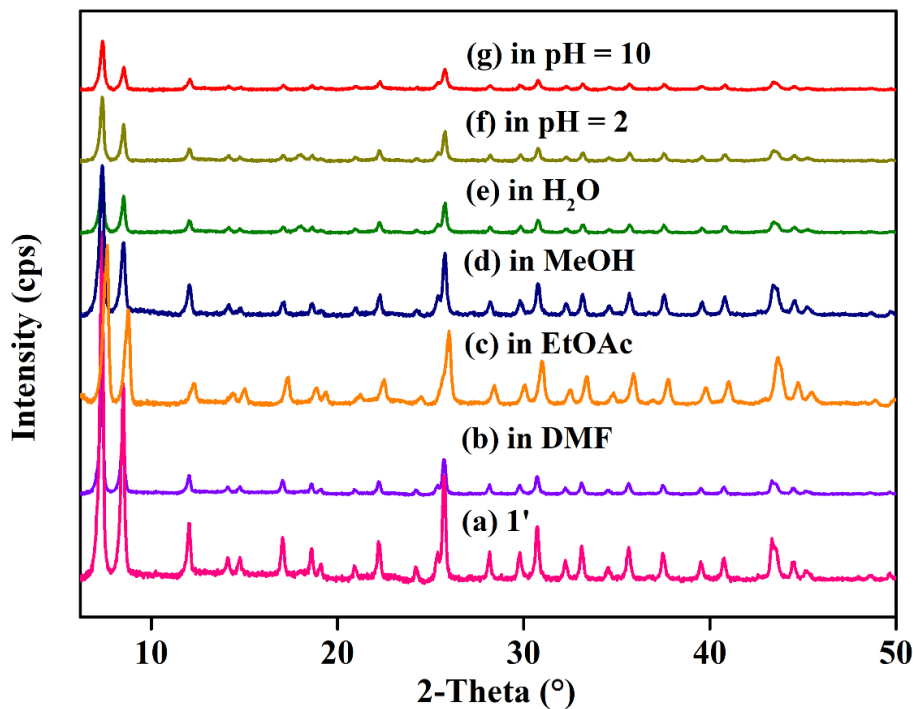
Figure S12. PXRD patterns of **1'** and the obtained samples of **1'** after stirring in different media.
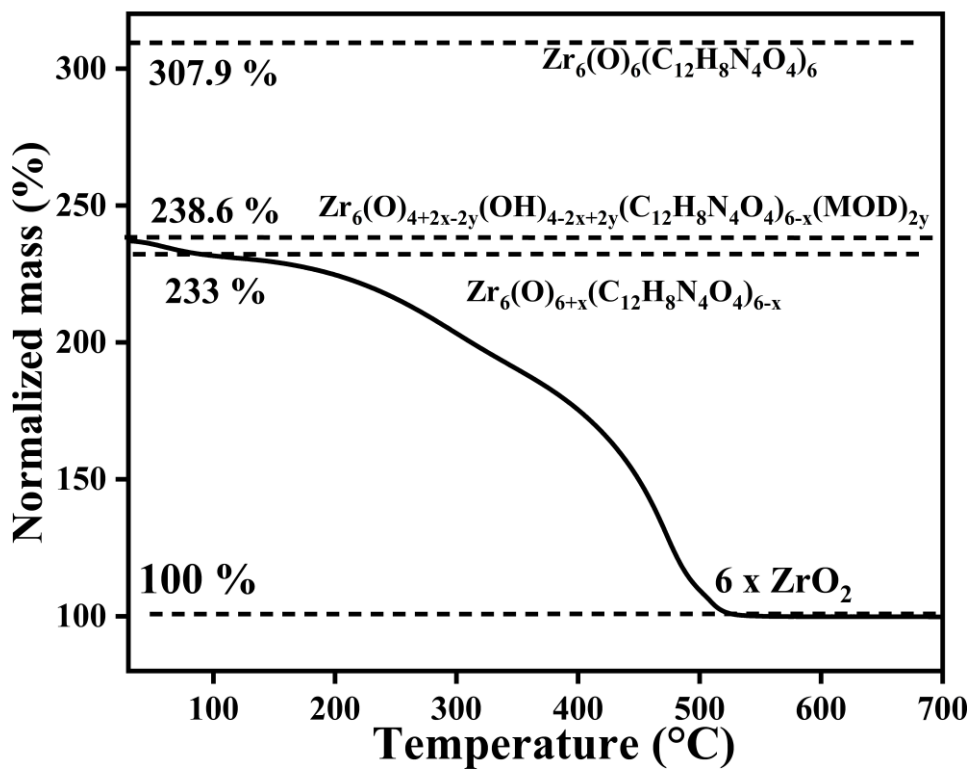
Figure S13. Calculation of missing ligand defects from the TG curve of activated **1'**. The vertical dashed line pinpoints $T_{Plat.}$, the temperature at which the plateau ($W_{Exp.\ Plat.}$) is reached. The horizontal dashed lines pinpoint the relevant TGA plateaus.

**Calculation of Linker Defects for 1' from TGA Data:**
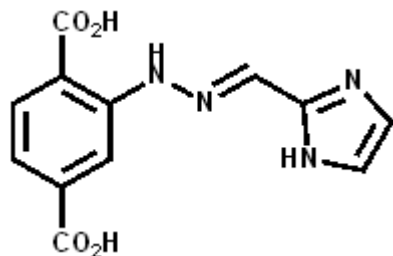
**2-(2-((1H-imidazol-2-yl)methylene)hydrazineyl)terephthalic acid**

Formula of MOF = $[Zr_6(O)_4(OH)_4(\mathbf{C_{12}H_8N_4O_4})_6]$

Molecular weight = 2312.7 g/mol

- ❖ The dehydroxylated and modulator free formula of MOF is $[Zr_6(O)_6(\mathbf{C_{12}H_8N_4O_4})_6]$ (ideal),
- ❖ Molecular Weight = 2276.6 g/mol
- ❖ The dehydroxylated and modulator free formula of MOF is $[Zr_6(O)_{6+x}(C_{10}H_{20}BrNO_6)_{6-x}]$ (experimental), Molecular Weight = 2276.6 g/mol (x = number of linker defect).
- ❖ From TGA data, after final weight loss step, the remaining mass is due to 6 moles of ZrO_2 i.e. $6 \times 123.2 = 739.3$ g/mol.
- ❖ The ideal weight of $[Zr_6(O)_6(\mathbf{C_{12}H_8N_4O_4})_6]$ is 3.08 times of 6 moles of ZrO_2.
- ❖ The remaining flat mass obtained at the last mass on TGA curve was normalized to 100%.
- ❖ The ideal normalized mass percentage for $[Zr_6(O)_6(\mathbf{C_{10}H_{20}BrNO_6})_6]$ is 308 %.
- ❖ The experimental normalized mass percentage of $[Zr_6(O)_{6+x}(C_{10}H_{20}BrNO_6)_{6-x}]$ from TGA is 233.06%.
- ❖ $x = 6 - (W_{wt.\ Plat} - W_{end}/Wt.PL._{Theo})$.

where

- ❖ $W_{wt.\ Plat}$ is the (normalized) weight of the sample at the second TGA plateau.
- ❖ W_{end} is 100 %
- ❖ $Wt.PL._{Theo} = (W_{wt.\ ideal\ Plat.} - W_{end})/NL_{ideal}$
- ❖ NL_{ideal} = number of linkers per unit formula ideally (6)
- ❖ $Wt.PL._{Theo} = ((308-100)/6) = 34.7$ %
- ❖ $x = 6 - ((233.06 - 100)/34.7) = 6 - 3.84 = 2.16$
- ❖ Number of linker defect per unit formula is 2.
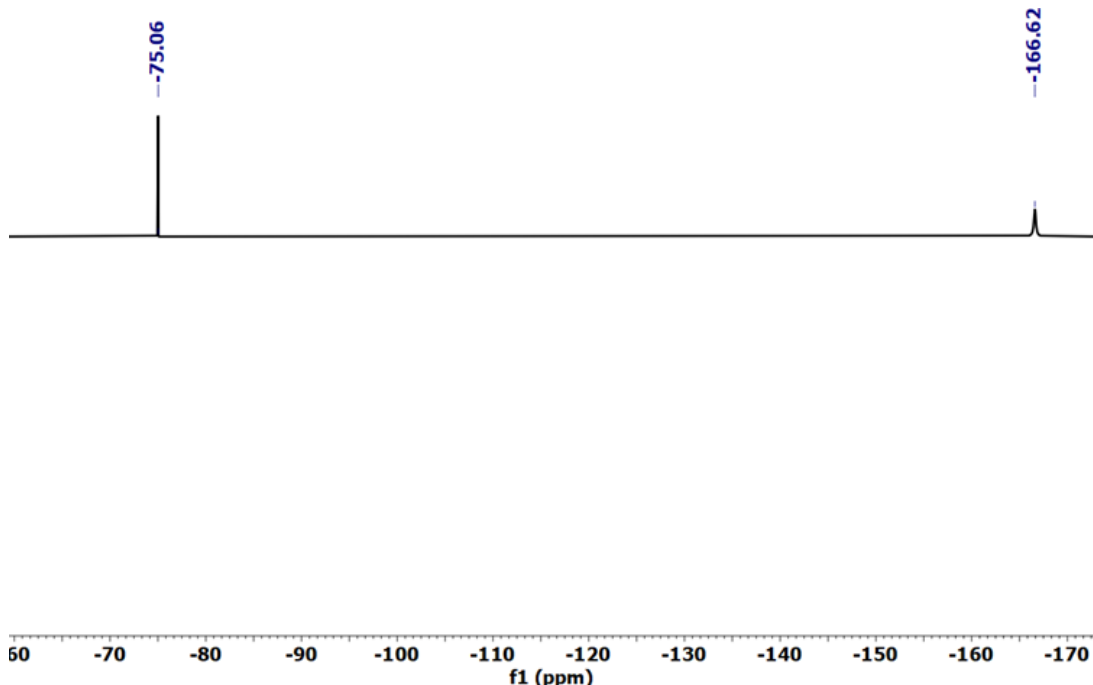
Figure S14. ^{19}F NMR spectrum of digested **1'** in DMSO-d6 with 40% HF.
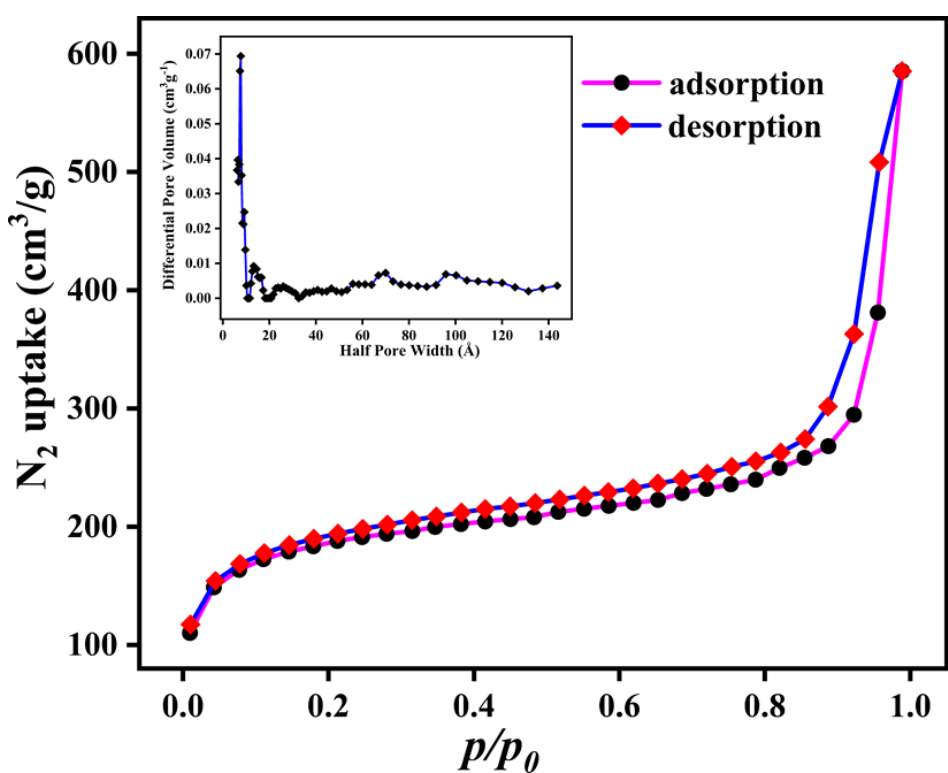
Figure S15. N$_2$ sorption isotherms of **1'** measured at -196 °C and density functional theory pore-size distribution of compound **1'** (shown in inset).
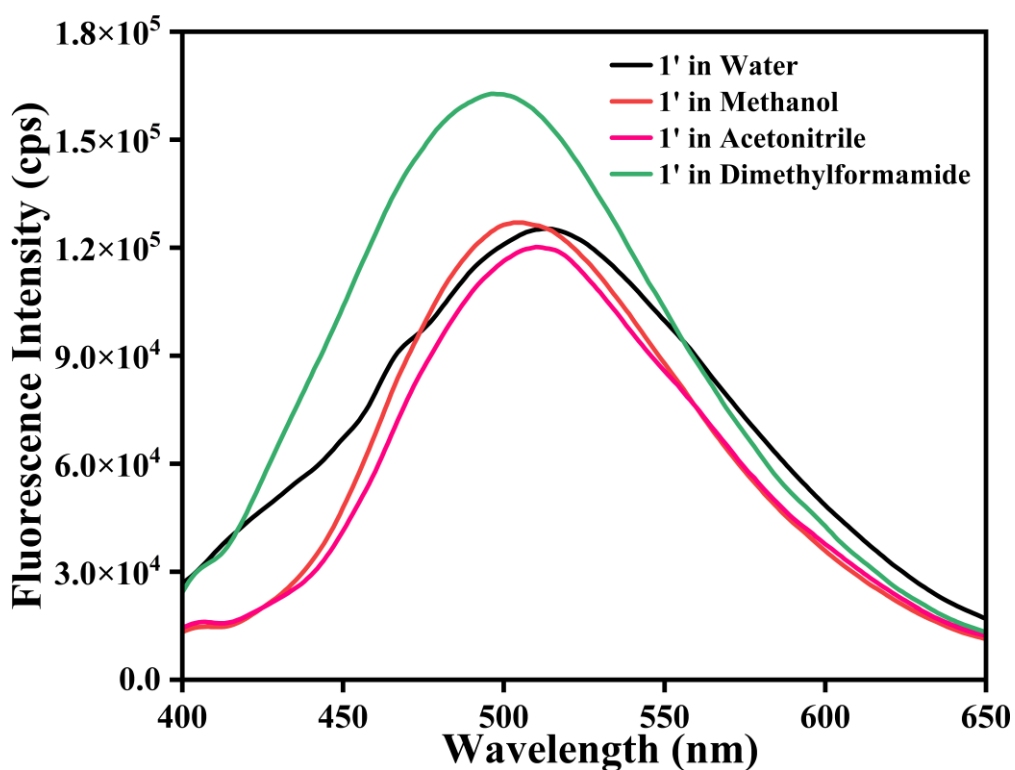
Figure S16. Fluorescence emission spectra of **1'** in different solvent media (H_2O, MeOH, acetonitrile and DMF).
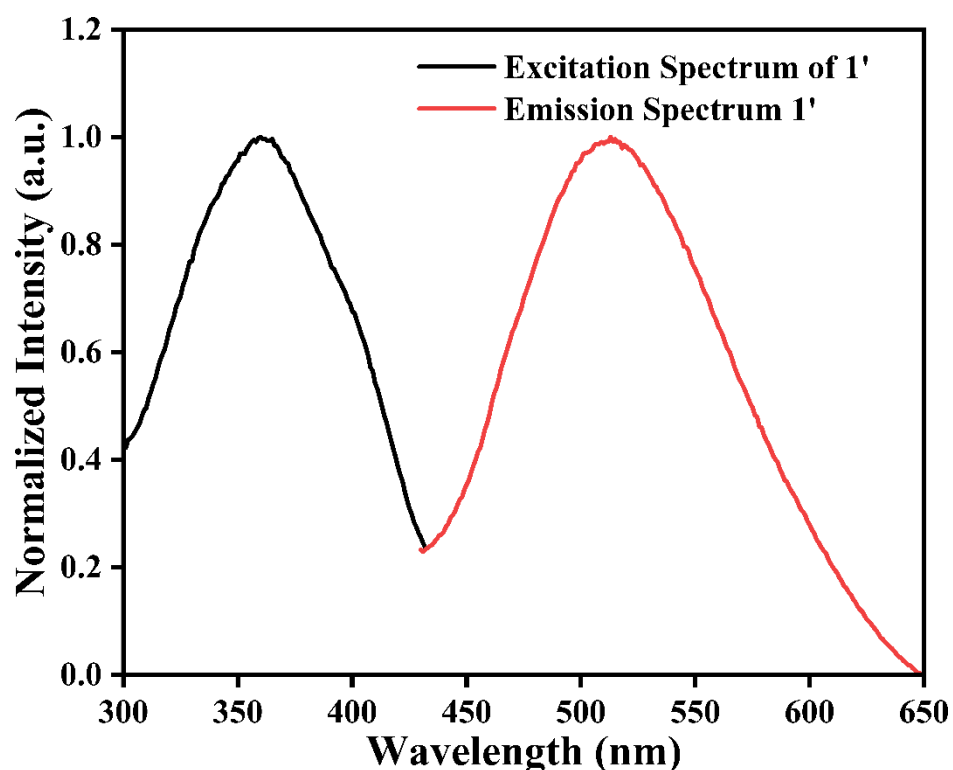
Figure S17. Fluorescence excitation and emission spectra of **1'** in water.
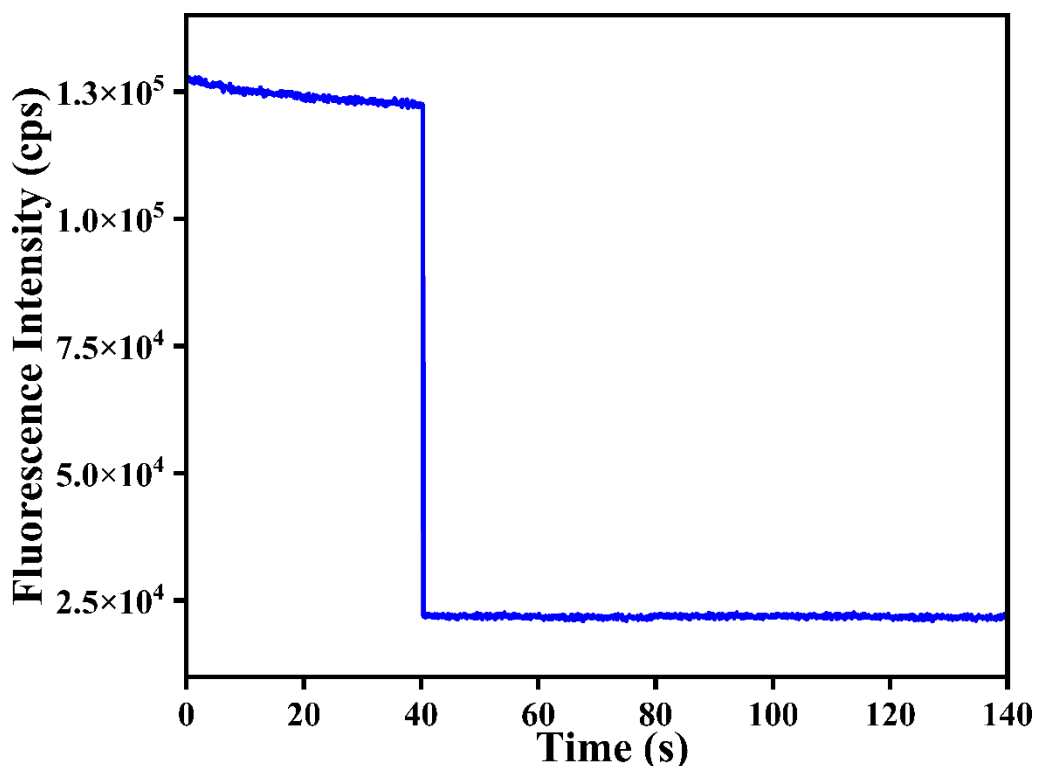
Figure S18. Fluorescence kinetic experiment for DNOC sensing.
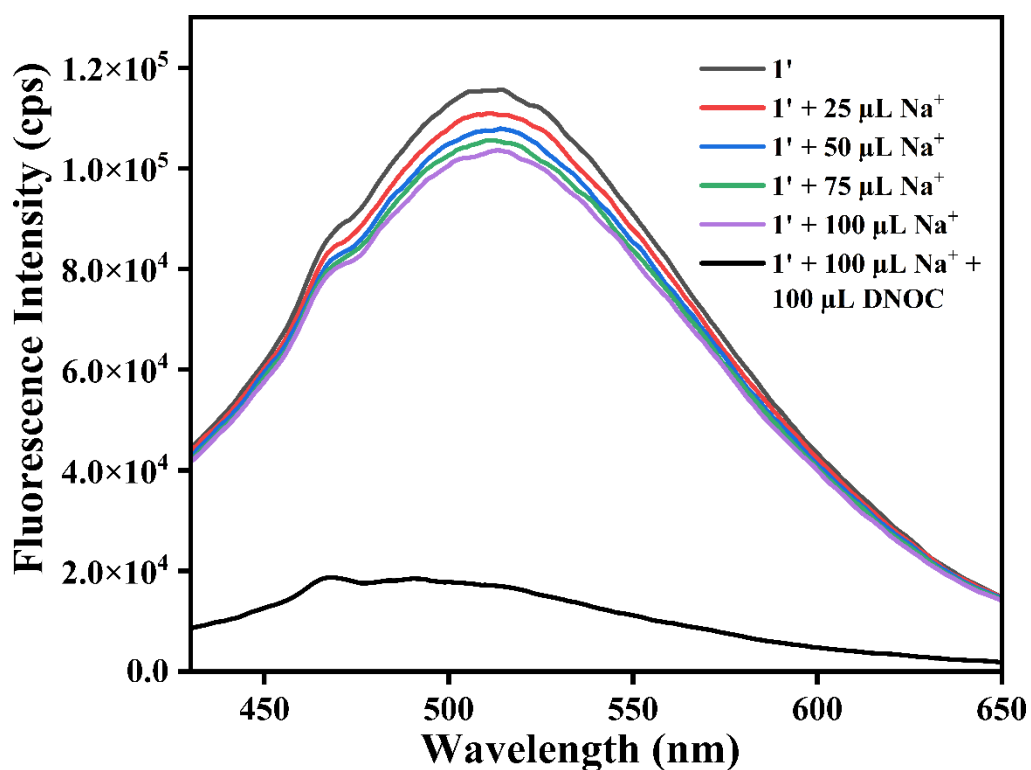
Figure S19. Fluorometric turn-off response of **1'** towards DNOC (100 µL, 5 mM) in the presence of Na$^+$ (100 µL, 5 mM).
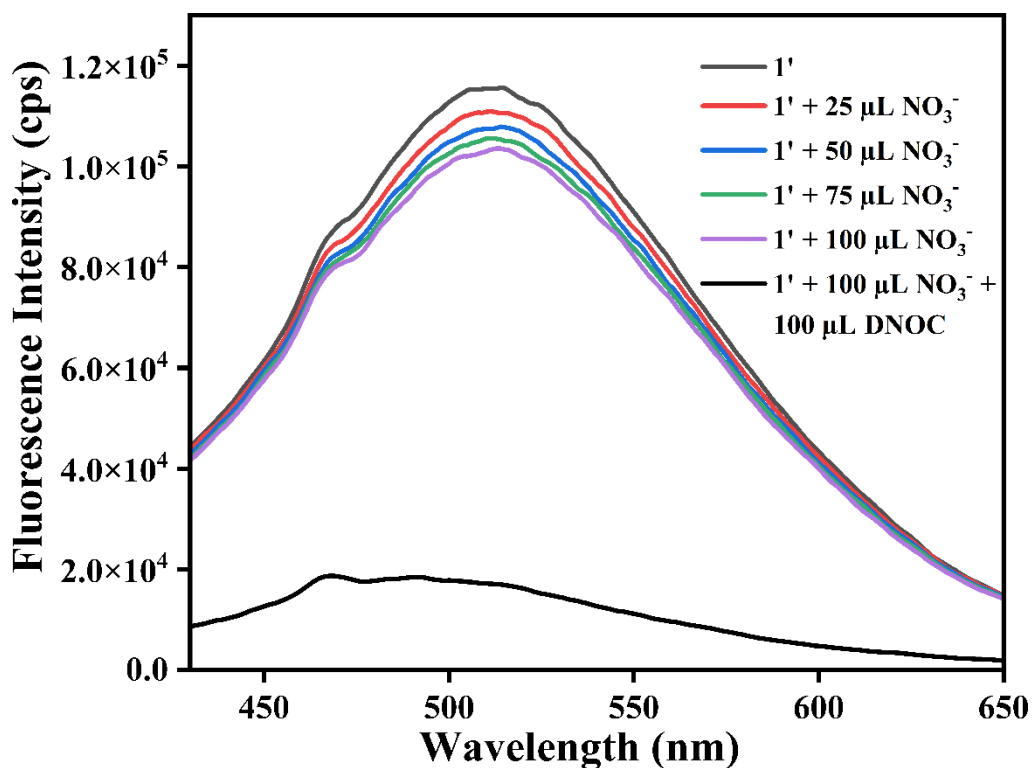
Figure S20. Fluorometric turn-off response of **1'** towards DNOC (100 µL, 5 mM) in the presence of NO_3^- (100 µL, 5 mM).
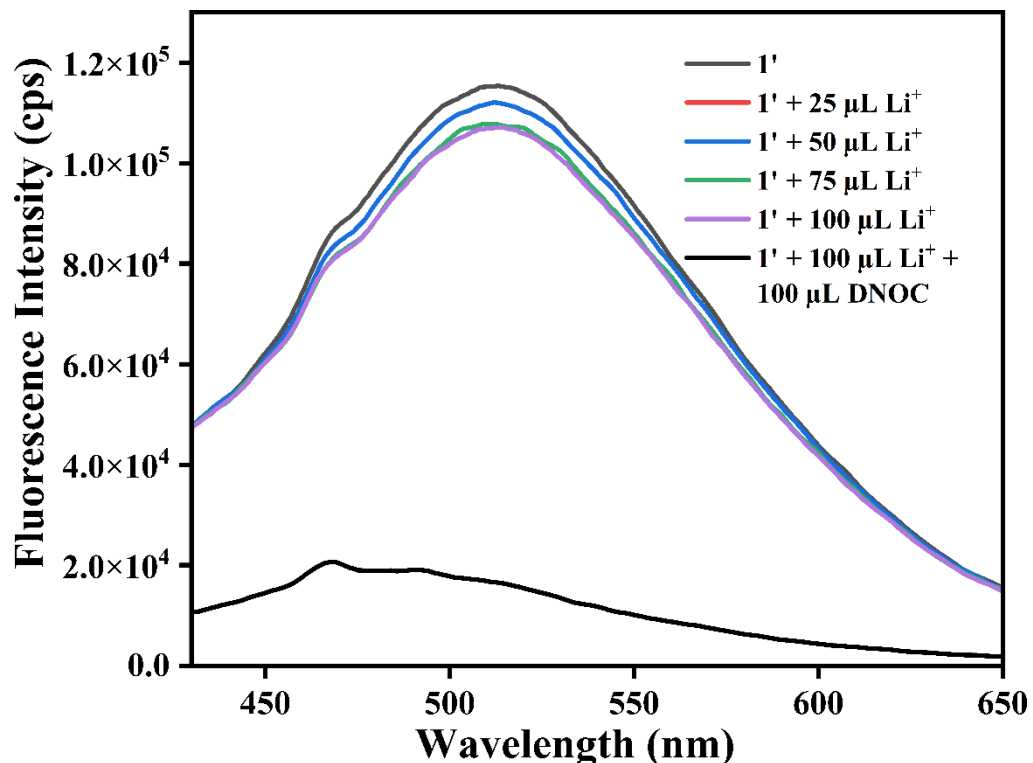
Figure S21. Fluorometric turn-off response of **1'** towards DNOC (100 µL, 5 mM) in the presence of Li^+ (100 µL, 5 mM).
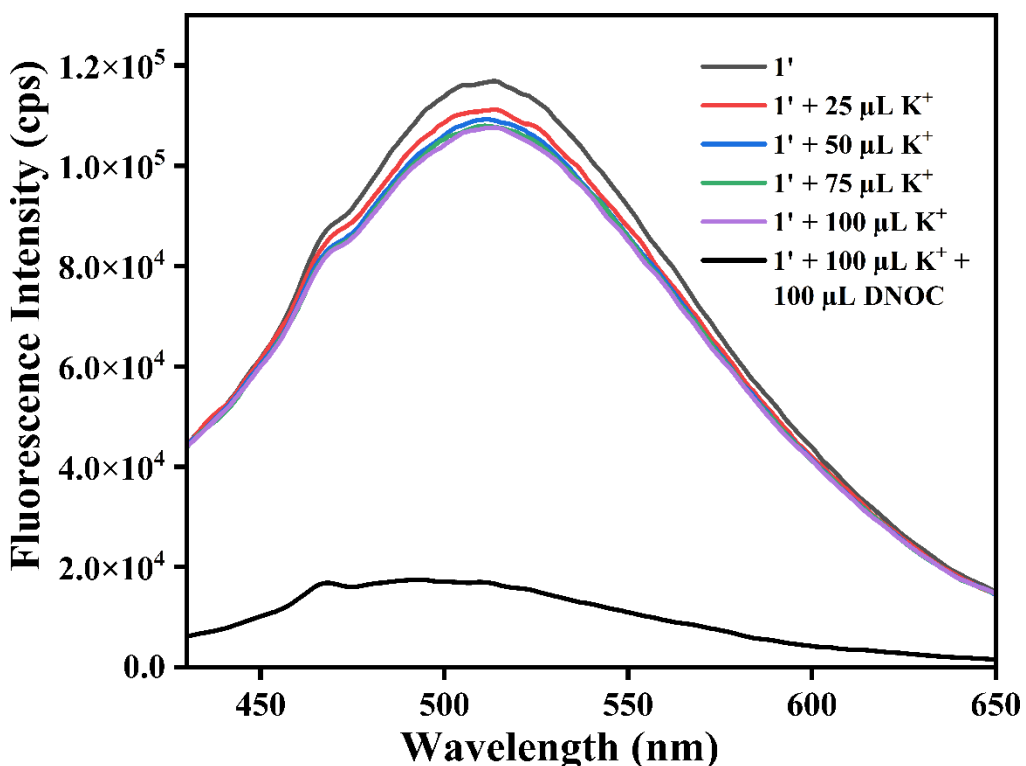
Figure S22. Fluorometric turn-off response of **1'** towards DNOC (100 µL, 5 mM) in the presence of K^+ (100 µL, 5 mM).
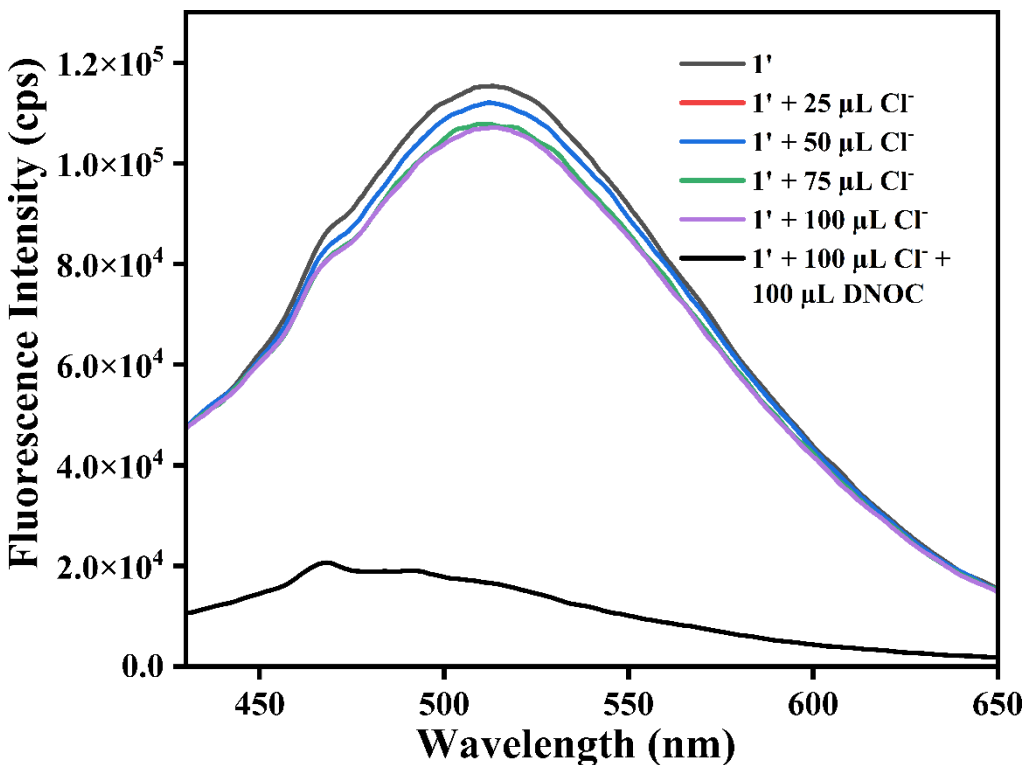
Figure S23. Fluorometric turn-off response of **1'** towards DNOC (100 µL, 5 mM) in the presence of Cl^- (100 µL, 5 mM).
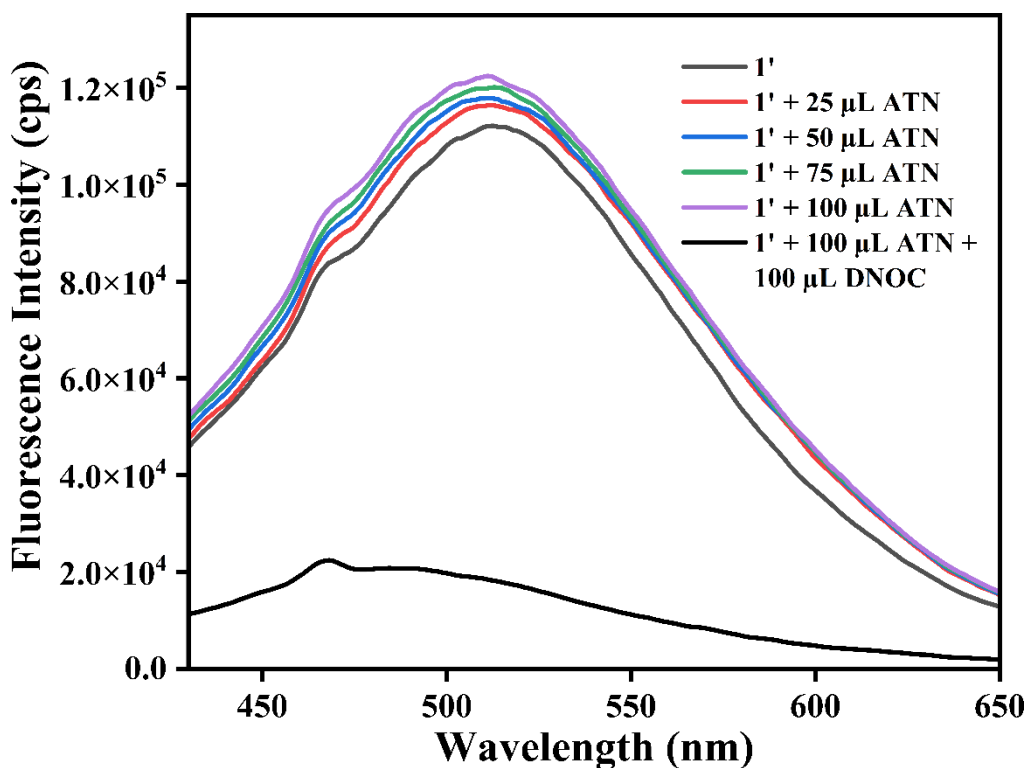
Figure S24. Fluorometric turn-off response of **1'** towards DNOC (100 μL, 5 mM) in the presence of atrazine (ATN) (100 μL, 5 mM).
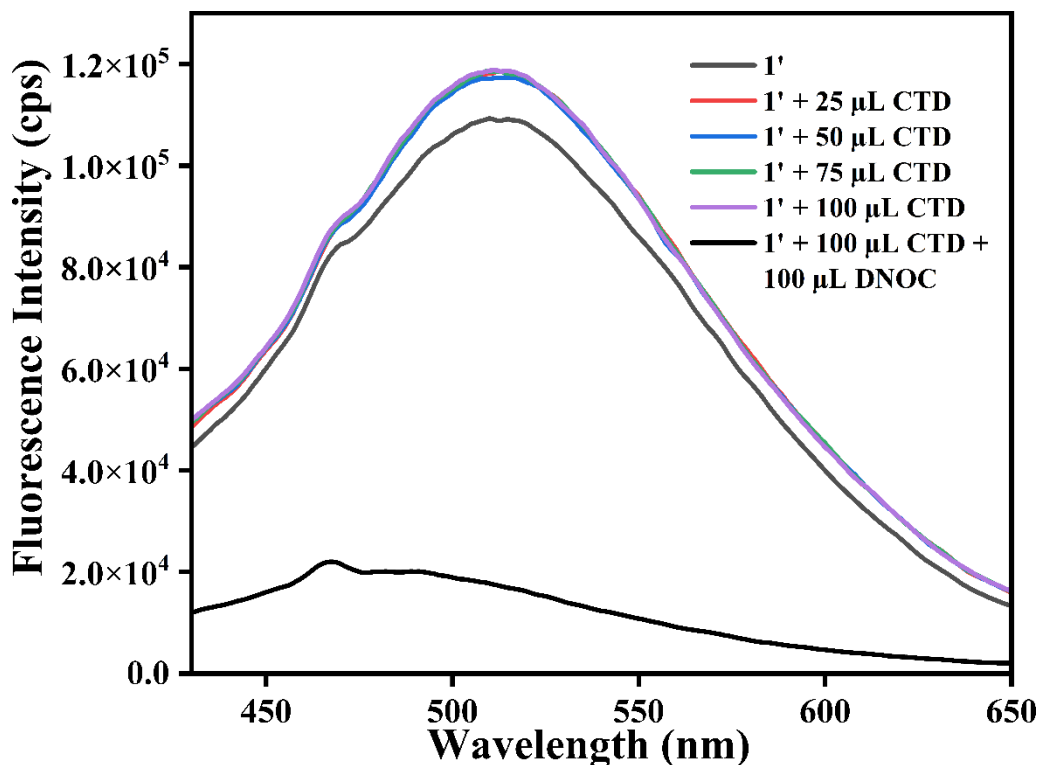
Figure S25. Fluorometric turn-off response of **1'** towards DNOC (100 μL, 5 mM) in the presence of clothianidin (CTD) (100 μL, 5 mM).
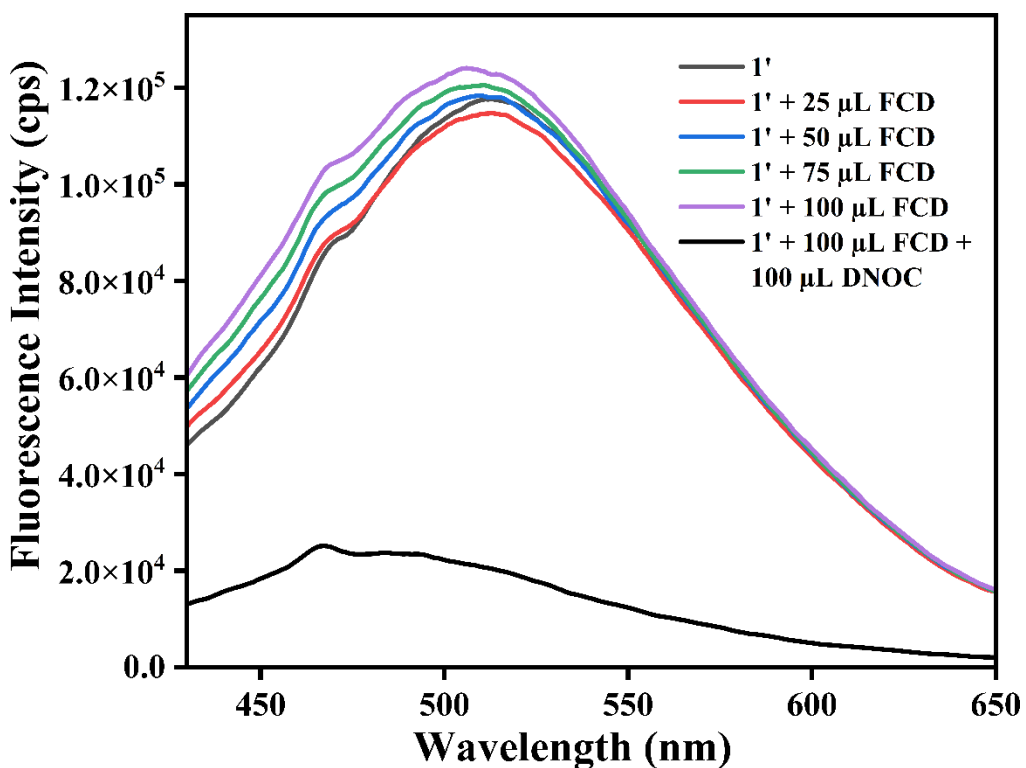
Figure S26. Fluorometric turn-off response of **1'** towards DNOC (100 μL, 5 mM) in the presence of flonicamid (FCD) (100 μL, 5 mM).
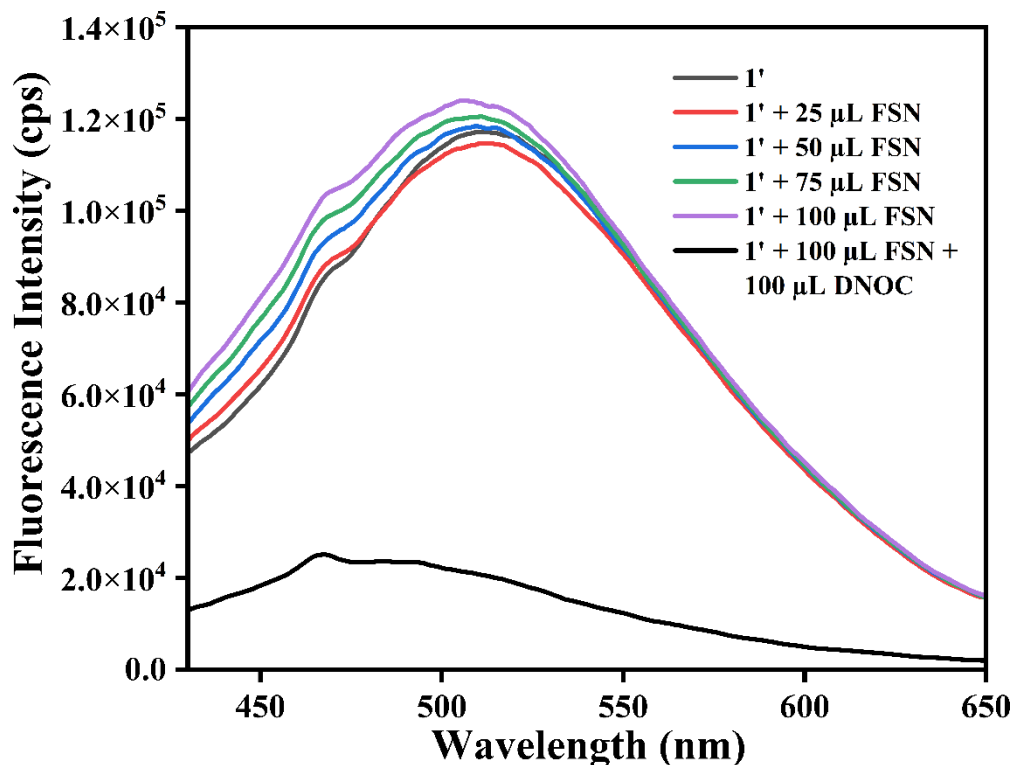
Figure S27. Fluorometric turn-off response of **1'** towards DNOC (100 μL, 5 mM) in the presence of fomesafen, (FSN) (100 μL, 5 mM).
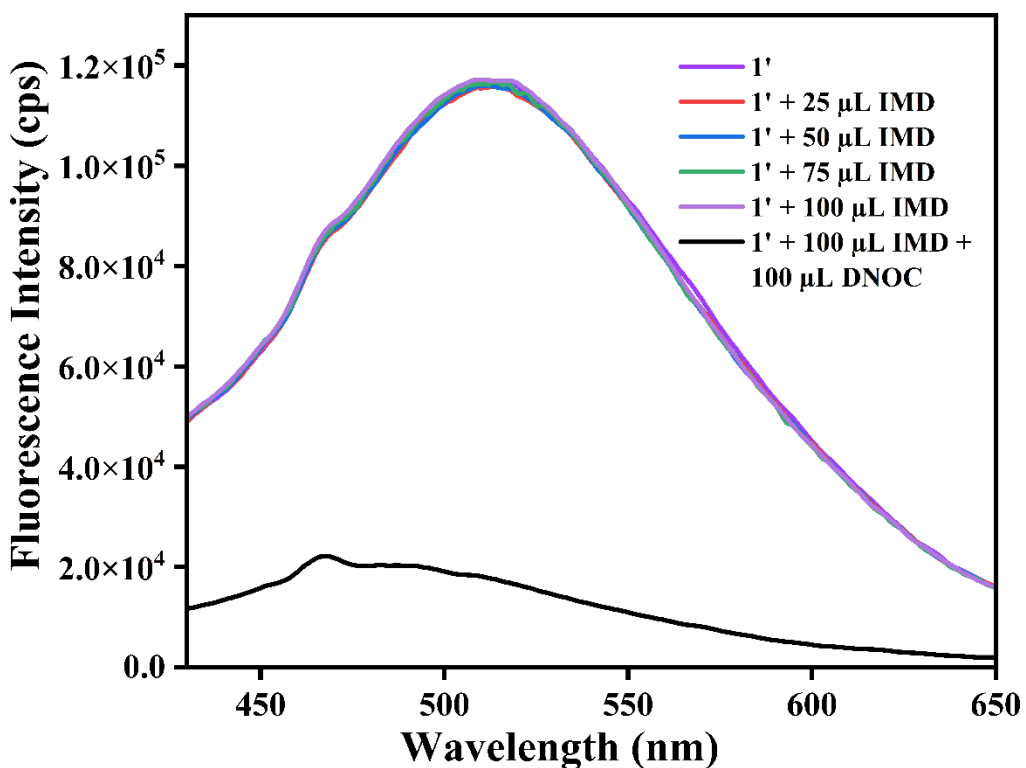
Figure S28. Fluorometric turn-off response of **1'** towards DNOC (100 µL, 5 mM) in the presence of imidacloprid (IMD) (100 µL, 5 mM).
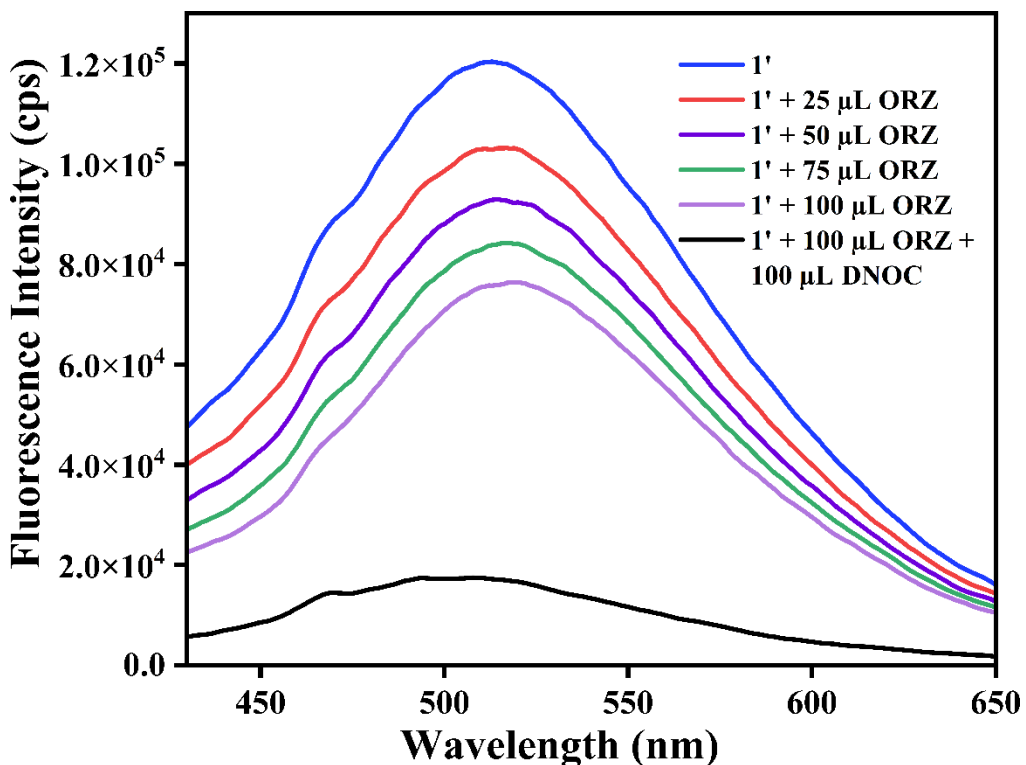
Figure S29. Fluorometric turn-off response of **1'** towards DNOC (100 µL, 5 mM) in the presence of oryzalin (ORZ) (100 µL, 5 mM).
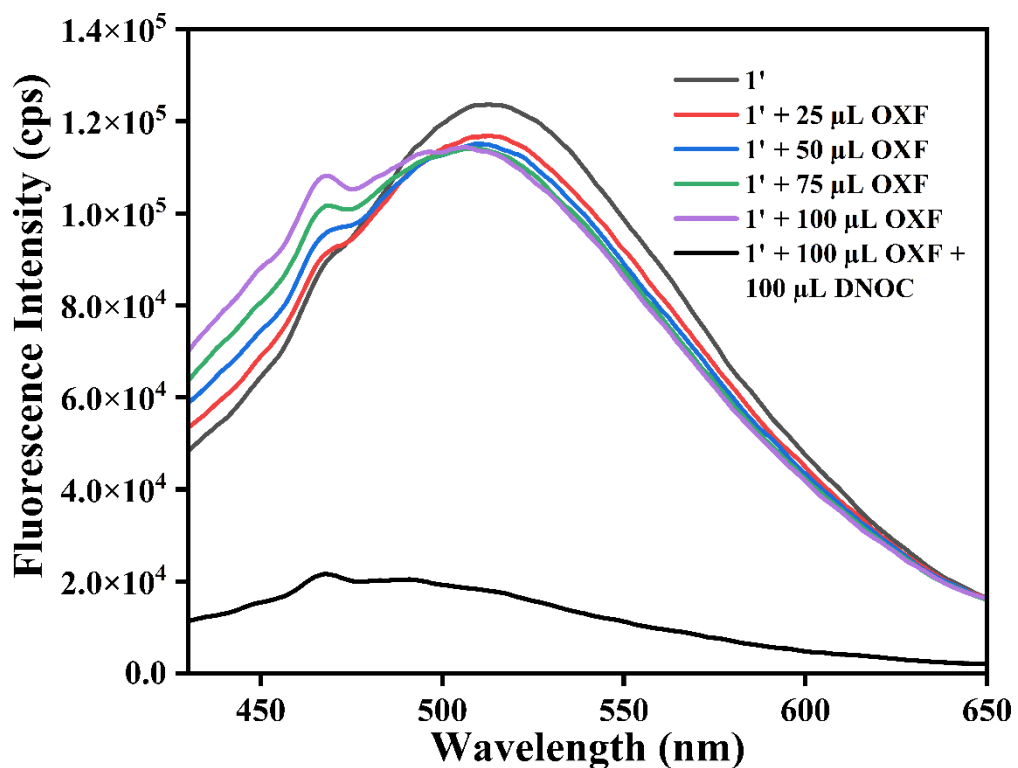
Figure S30. Fluorometric turn-off response of **1'** towards DNOC (100 µL, 5 mM) in the presence of oxyfluorfen (OXF) (100 µL, 5 mM).
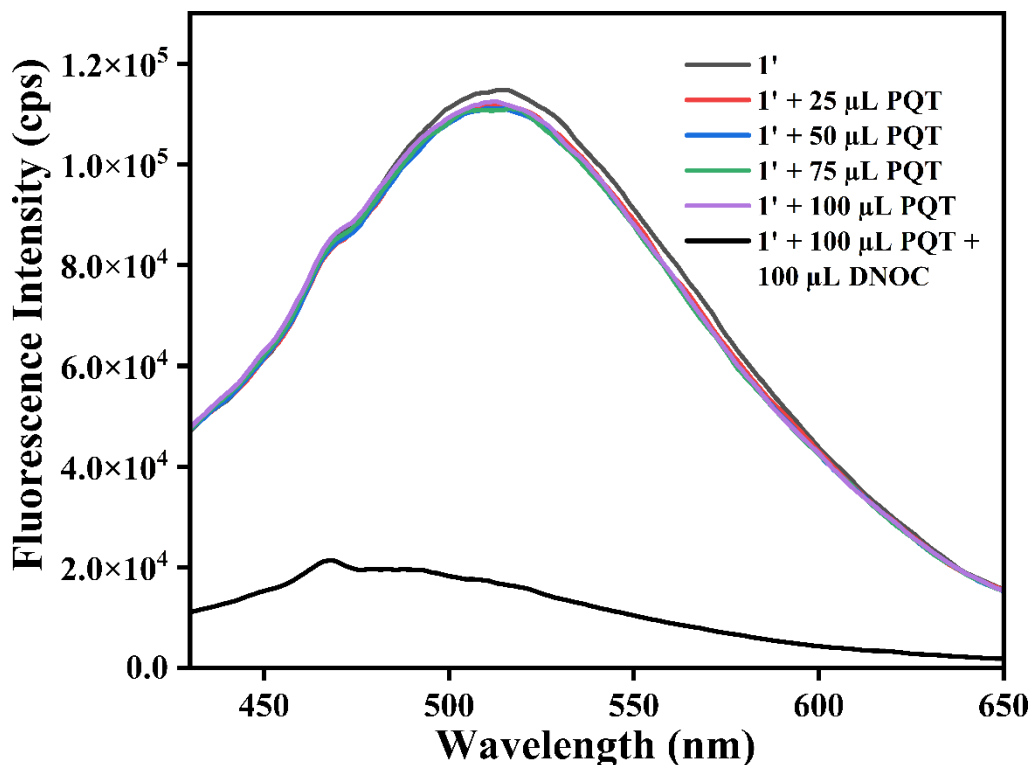
Figure S31. Fluorometric turn-off response of **1'** towards DNOC (100 µL, 5 mM) in the presence of paraquat, (PQT) (100 µL, 5 mM).
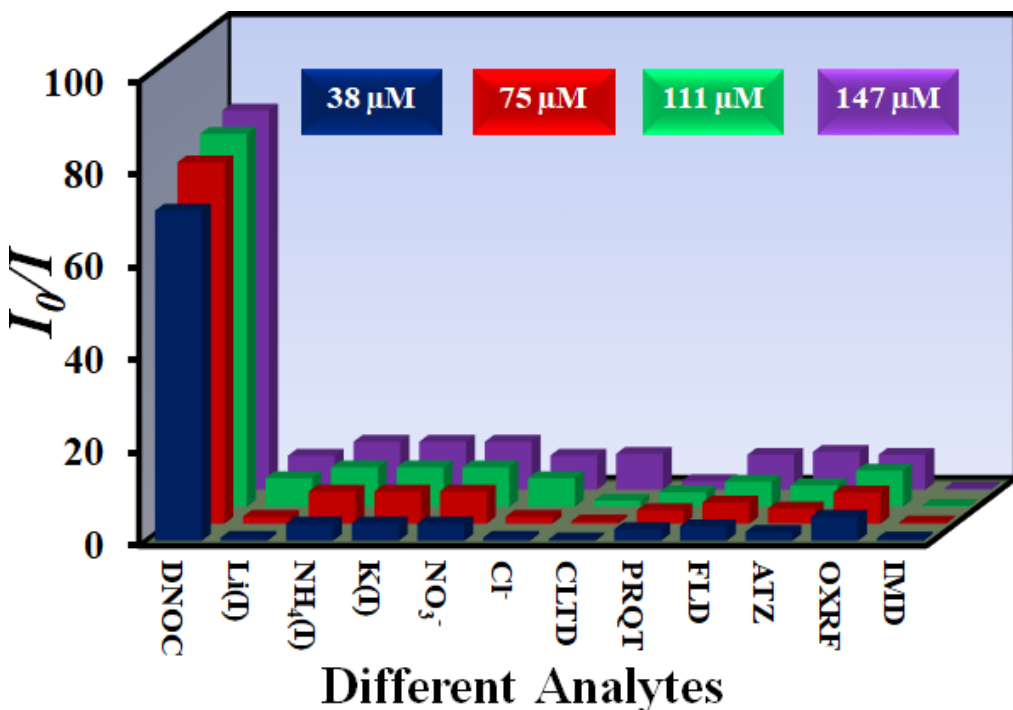
Figure S32. 3-D Stern-Volmer plots for DNOC sensing.

Table S3. Evaluation of intra-day, inter-day accuracy and precision study of change in fluorescence intensity of **1′** after incremental addition of 5 mM aqueous solution of DNOC.

Type of Precision	Amount of DNOC Added (µL)	Fluorescence Intensity			Average PL Intensity (cps)	SD	Error	RSD (%)
Intra Day	0	125829.0	125634.8	125021.1	125495.0	421.7	-0.003	-0.3
	25	21805.2	21800.5	21711.1	21772.2	53.0	-0.002	-0.2
	50	18755.6	18522.3	18305.5	18527.8	225.1	-0.012	-1.2
	75	18205.1	18407.1	18284.7	18298.9	101.7	0.005	0.5
	100	18628.1	18557.4	18071.7	18419.1	302.9	-0.011	-1.1
Inter Day	0	125021.1	125085.2	124843.9	124983.4	125.0	0.000	0.0
	25	21711.1	21474.1	21395.9	21527.0	164.1	-0.008	-0.8
	50	18305.5	18159.2	18037.1	18167.3	134.4	-0.008	-0.8
	75	18284.7	18012.6	17836.2	18044.5	225.9	-0.013	-1.3
	100	18071.7	18200.9	17865.5	18046.0	169.2	-0.001	-0.1
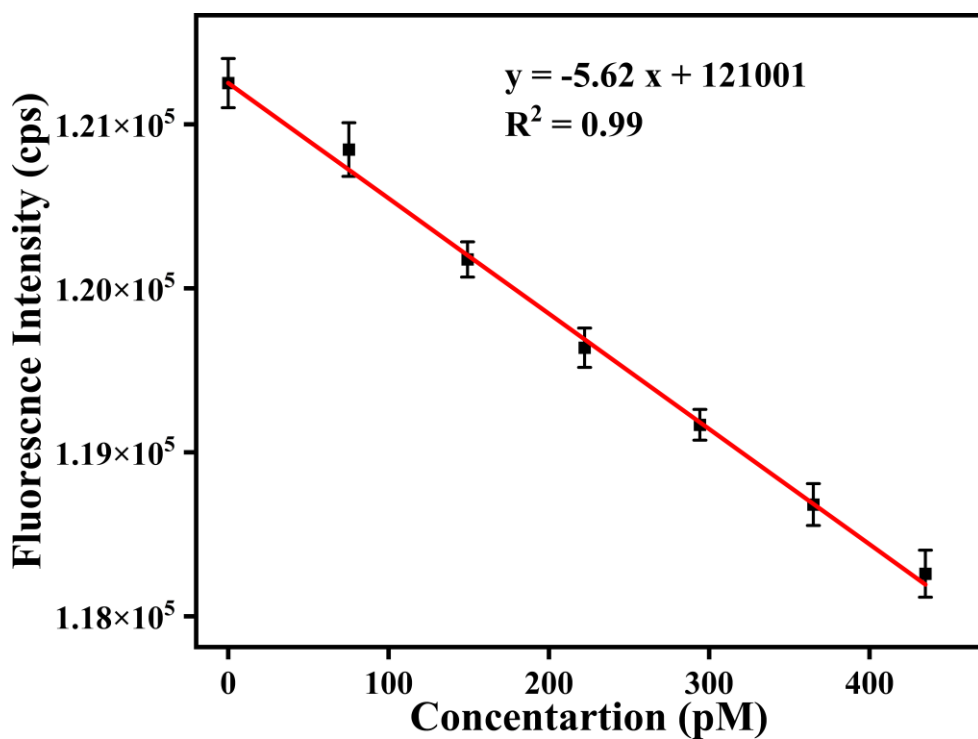
Figure S33. Change in the fluorescence intensity of **1'** in water as a function of concentration of DNOC (black colour error bars signify the standard deviations of three individual measurements).
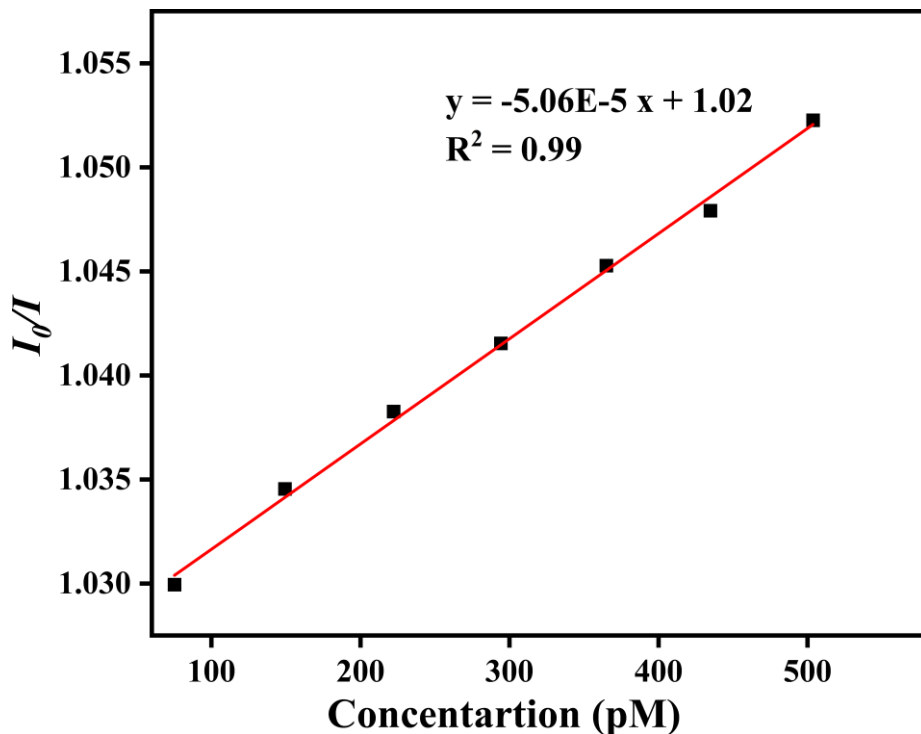
Figure S34. Stern-Volmer plot for the fluorescence quenching of **1'** in presence of DNOC in aqueous medium (black colour error bars signify the standard deviations of three individual measurements).
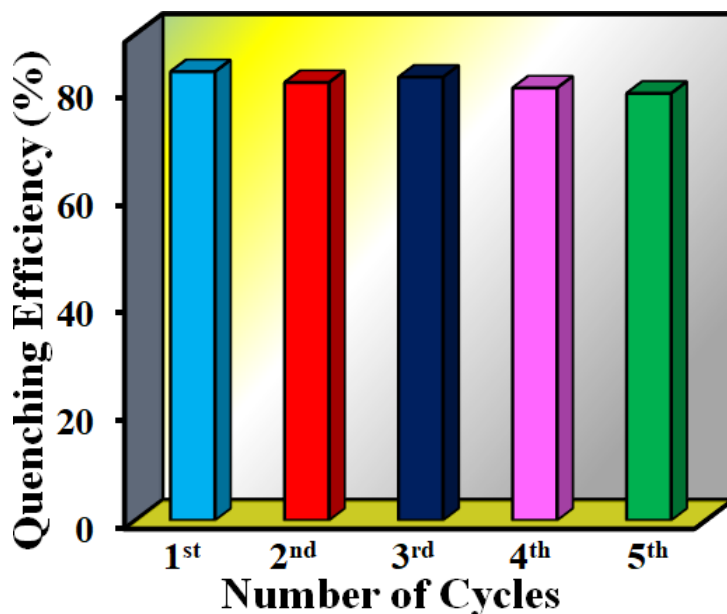
Figure S35. Reusability of probe **1'** towards DNOC sensing in aqueous medium.

Table S4. Fluorescence lifetimes of **1′** before and after the addition of DNOC solution (λ_{ex} = 375 nm, pulsed diode laser).

Volume of DNOC Solution Added (μL)	α_1	τ_1 (ns)	$<\tau>*$ (ns)	χ^2
0	1	12.5	15.20	1.12
100	1	6.1	6.1	0.97

$<\tau>* = \alpha_1\tau_1$
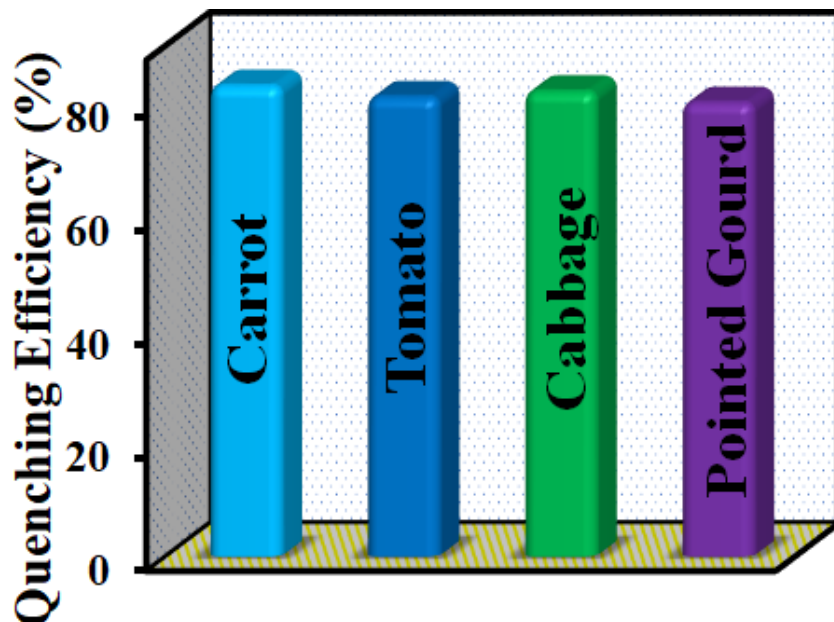
Figure S36. Detection of DNOC in different fruits and vegetables extracts using probe **1'**.
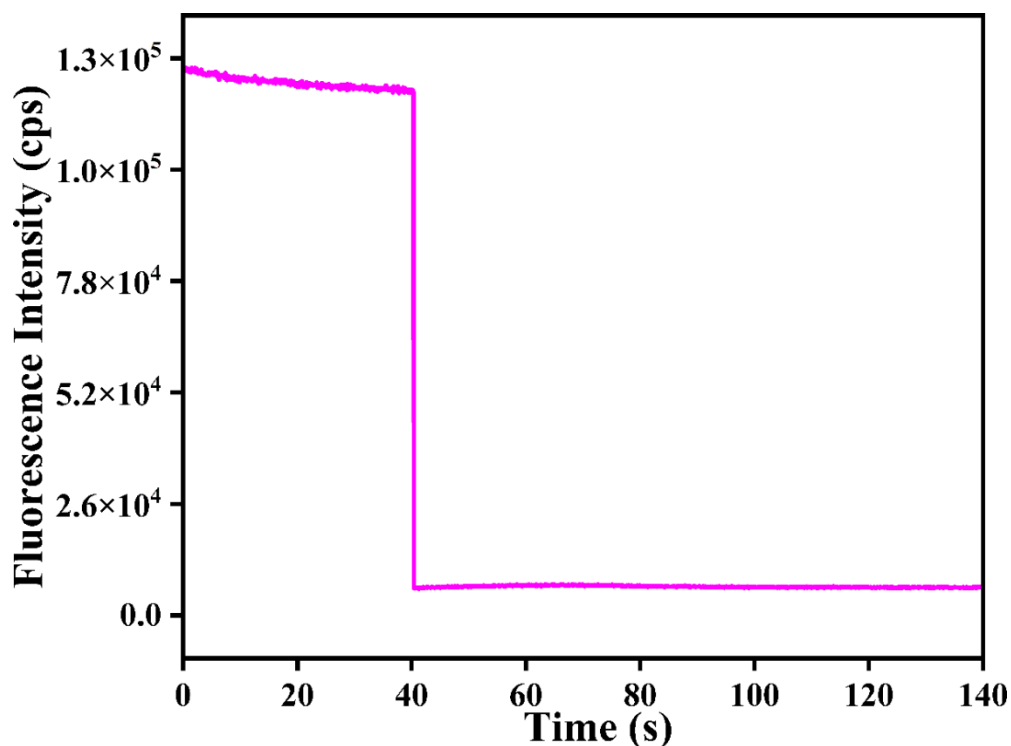
Figure S37. Fluorescence kinetic experiment for furaltadone (FLT) sensing.
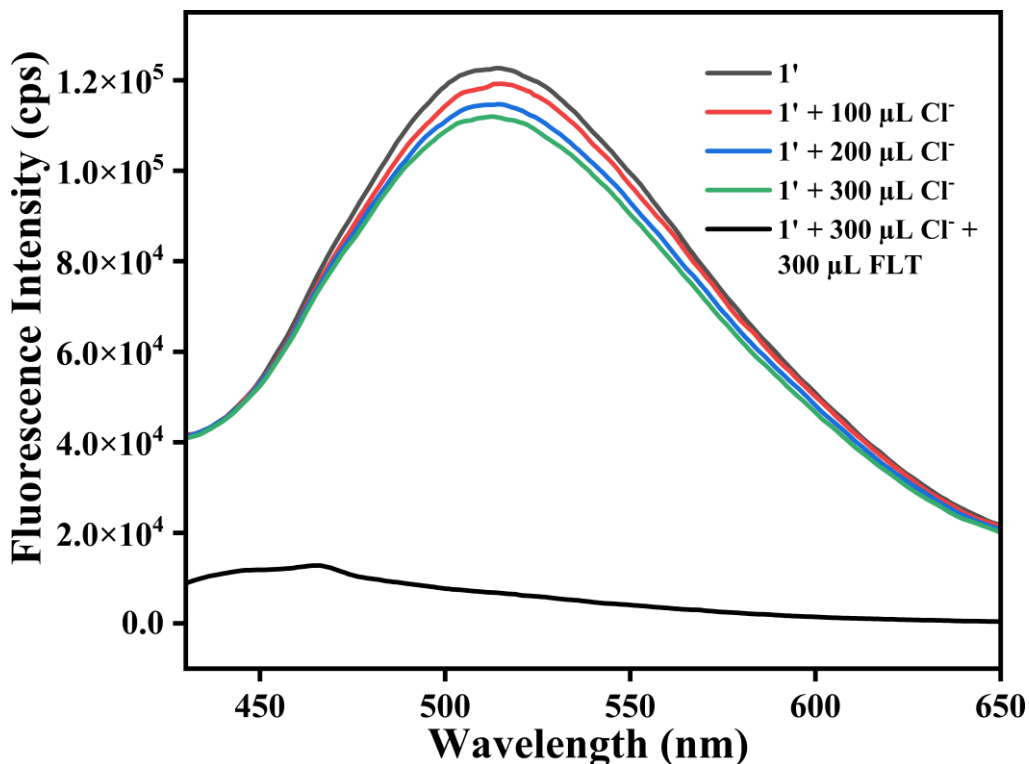
Figure S38. Fluorometric turn-off response of **1'** towards furaltadone (FLT) (300 μL, 5 mM) in the presence of Cl⁻ (300 μL, 5 mM).
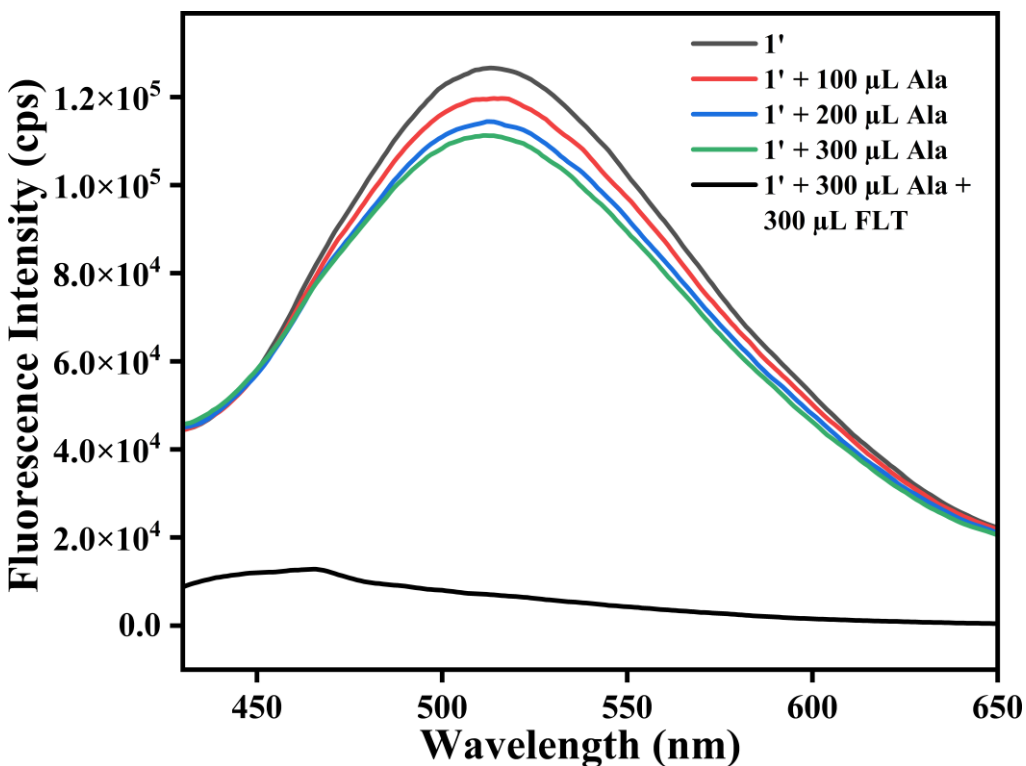
Figure S39. Fluorometric turn-off response of **1'** towards furaltadone (FLT) (300 μL, 5 mM) in the presence of alanine (Ala) (300 μL, 5 mM).
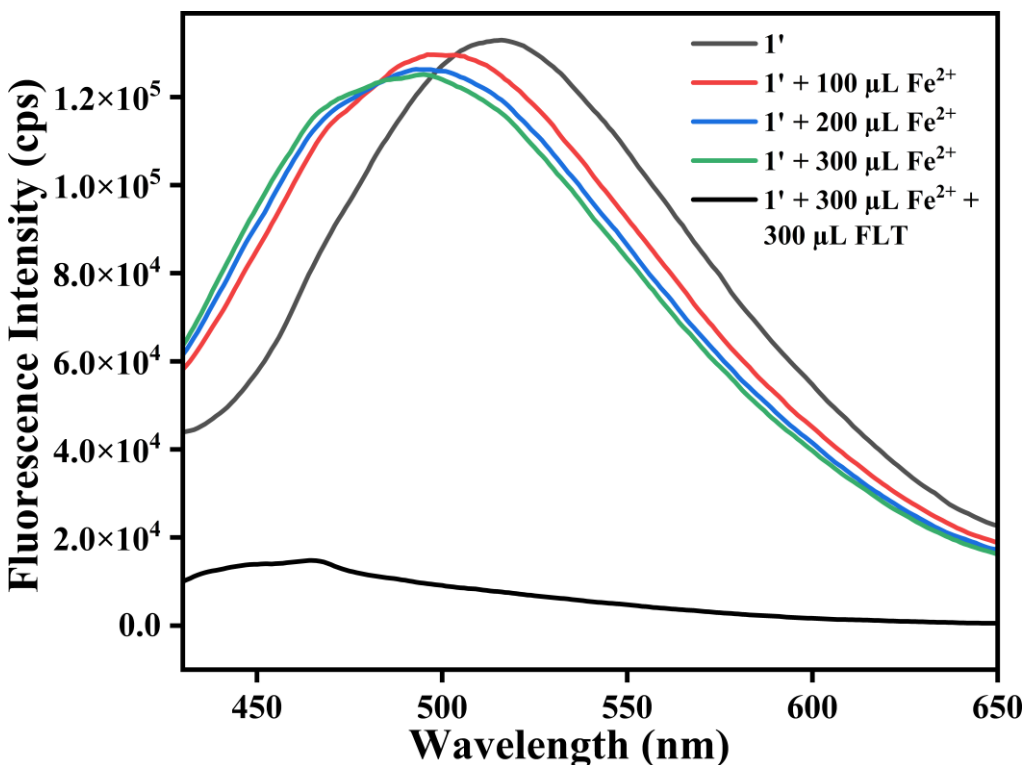
Figure S40. Fluorometric turn-off response of **1'** towards furaltadone (FLT) (300 μL, 5 mM) in the presence of Fe^{2+} (300 μL, 5 mM).
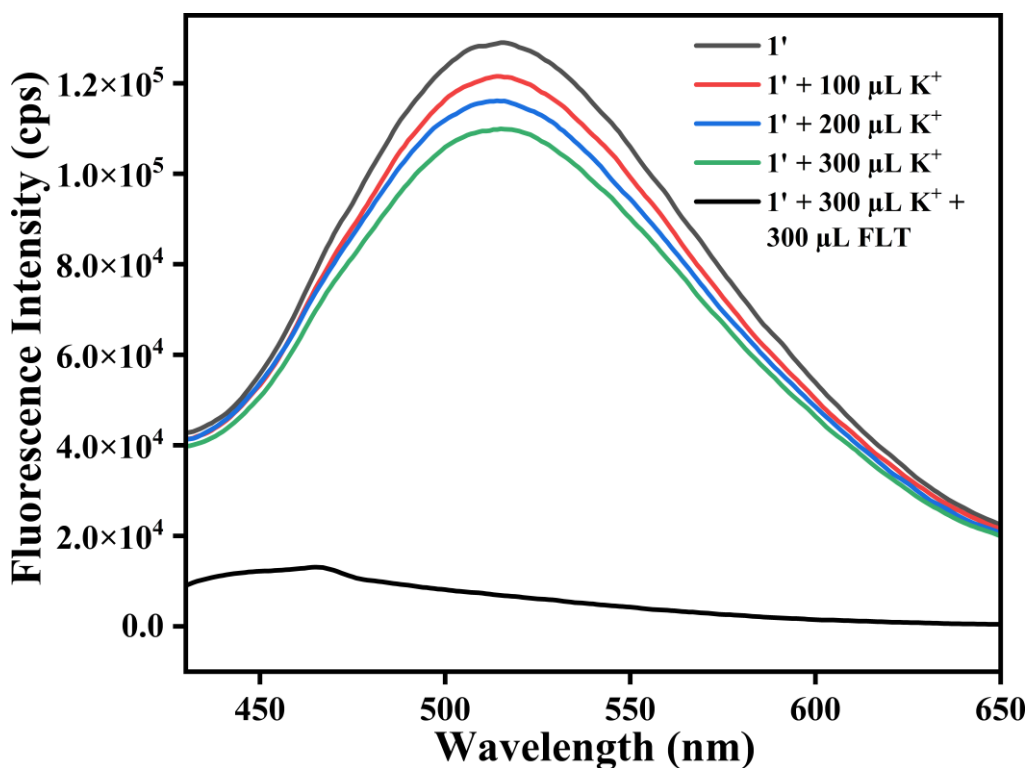
Figure S41. Fluorometric turn-off response of **1'** towards furaltadone (FLT) (300 μL, 5 mM) in the presence of K^+ (300 μL, 5 mM).
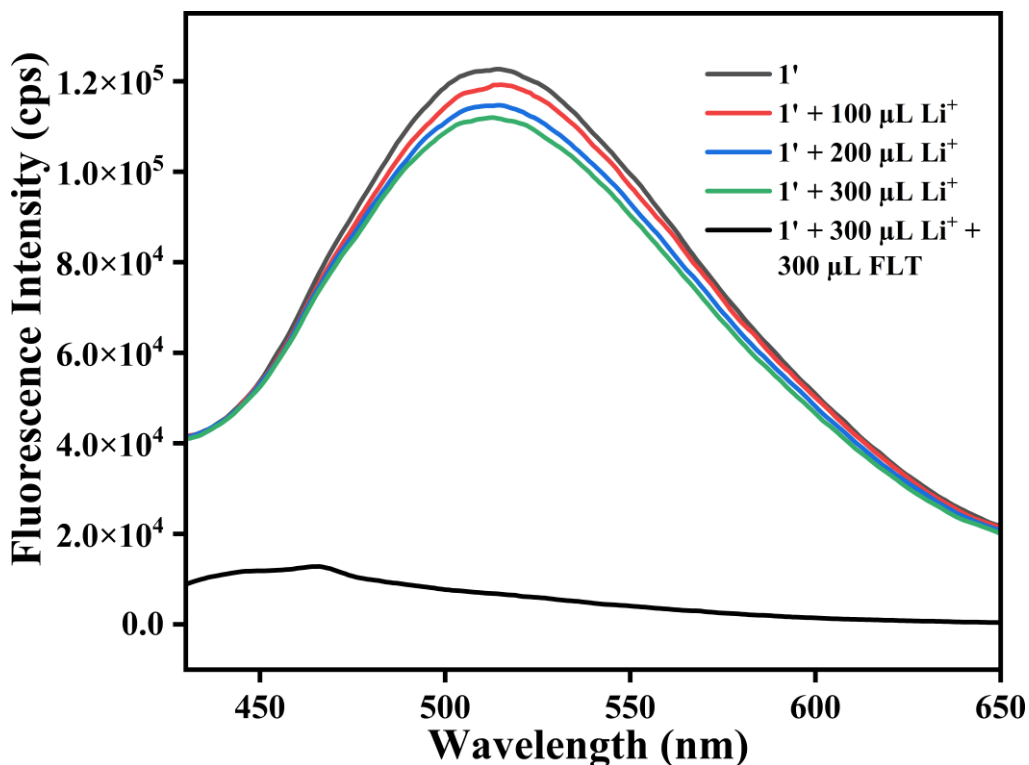
Figure S42. Fluorometric turn-off response of **1'** towards furaltadone (FLT) (300 μL, 5 mM) in the presence of Li^+ (300 μL, 5 mM).
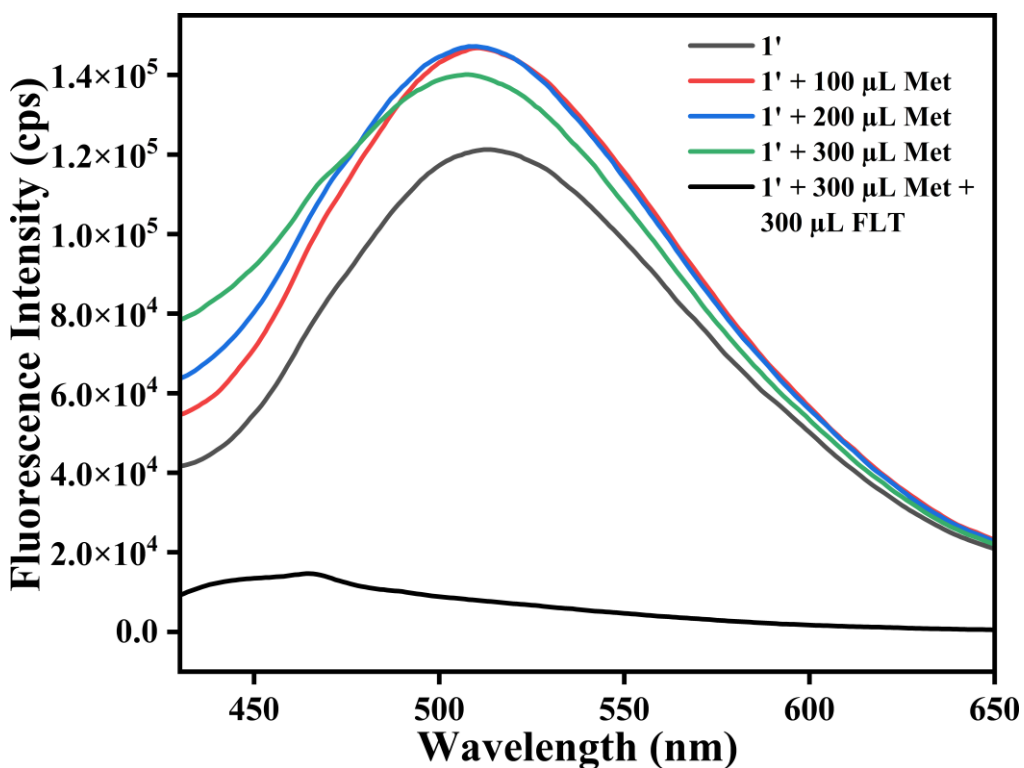
Figure S43. Fluorometric turn-off response of **1'** towards furaltadone (FLT) (300 μL, 5 mM) in the presence of methionine (Met) (300 μL, 5 mM).
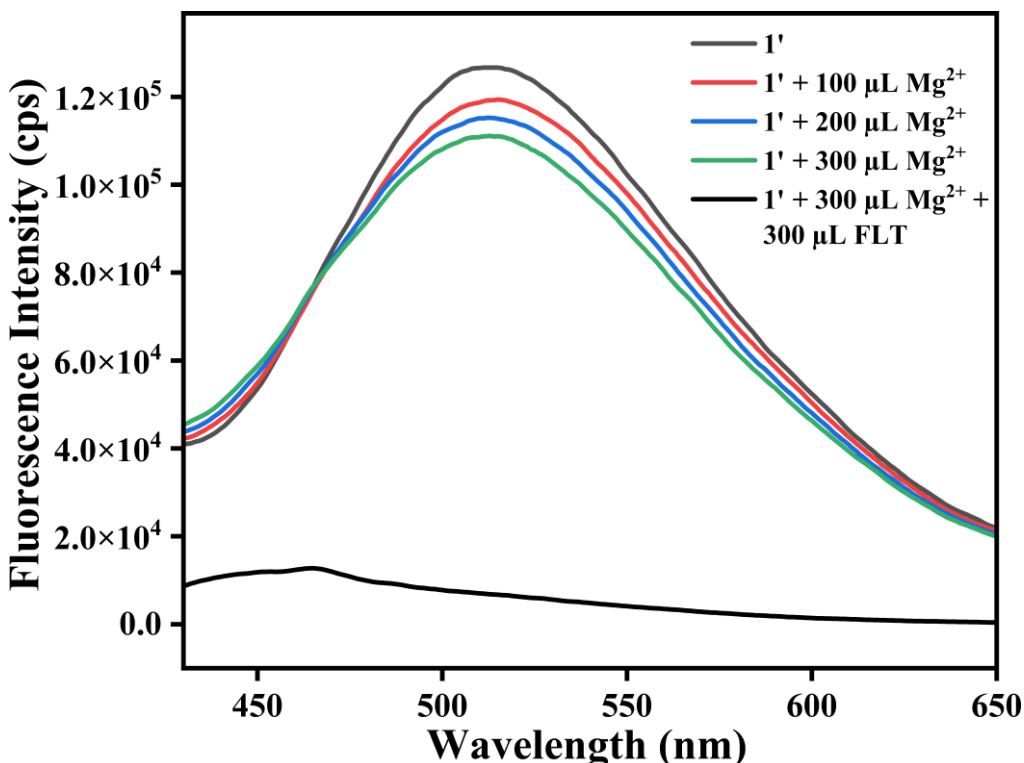
Figure S44. Fluorometric turn-off response of **1'** towards furaltadone (FLT) (300 μL, 5 mM) in the presence of Mg^{2+} (300 μL, 5 mM).
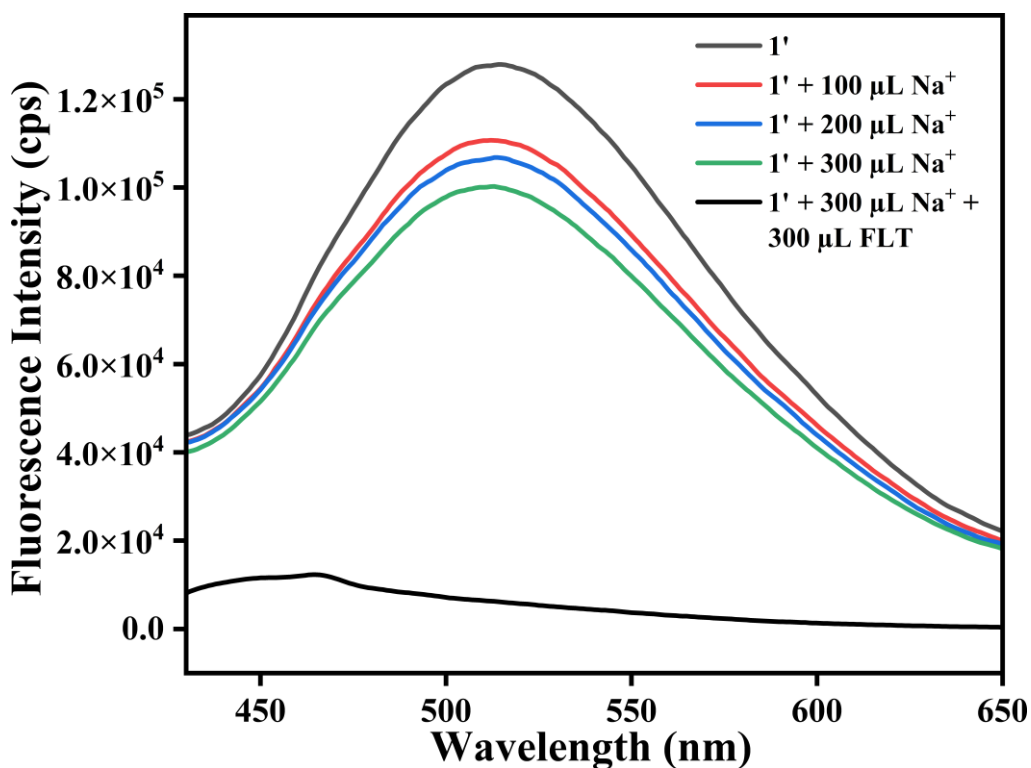
Figure S45. Fluorometric turn-off response of **1'** towards furaltadone (FLT) (300 μL, 5 mM) in the presence of Na^+ (300 μL, 5 mM).
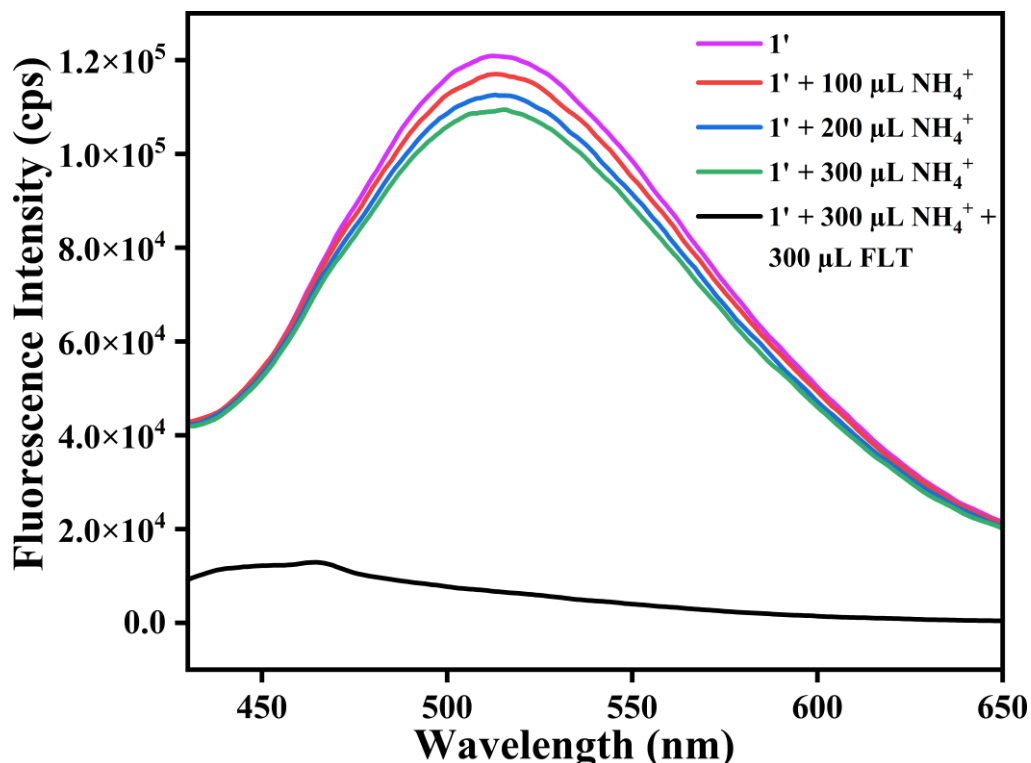
Figure S46. Fluorometric turn-off response of **1'** towards furaltadone (FLT) (300 μL, 5 mM) in the presence of NH_4^+ (300 μL, 5 mM).
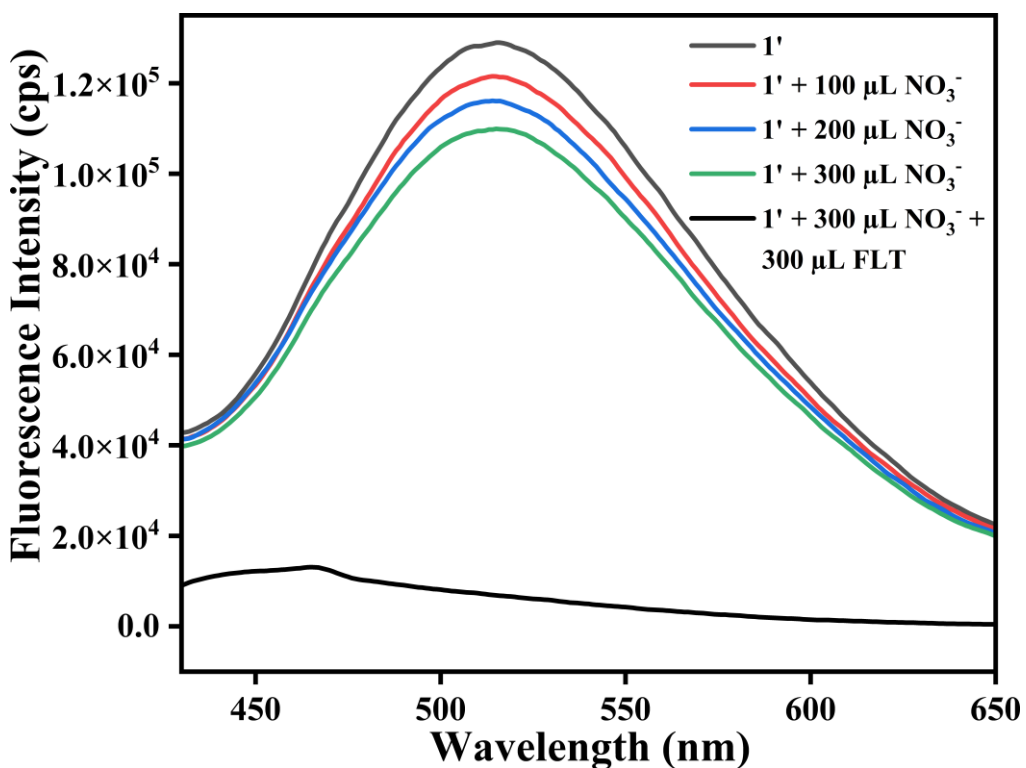
Figure S47. Fluorometric turn-off response of **1'** towards furaltadone (FLT) (300 μL, 5 mM) in the presence of NO_3^- (300 μL, 5 mM).
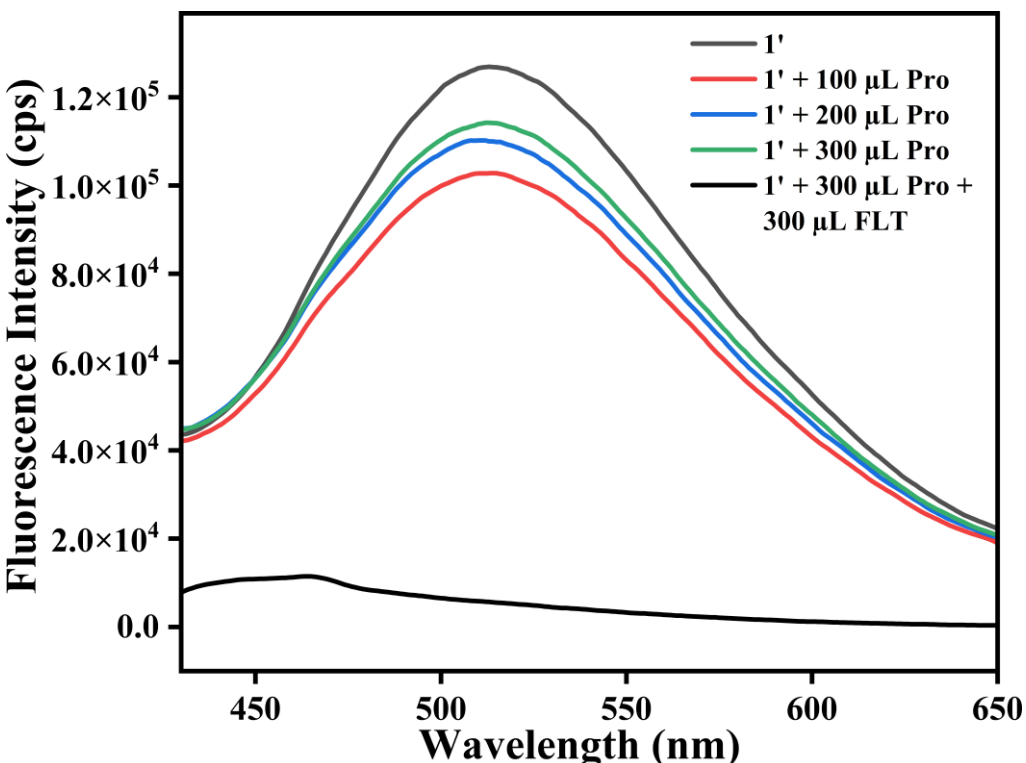
Figure S48. Fluorometric turn-off response of **1'** towards furaltadone (FLT) (300 μL, 5 mM) in the presence of proline (Pro) (300 μL, 5 mM).
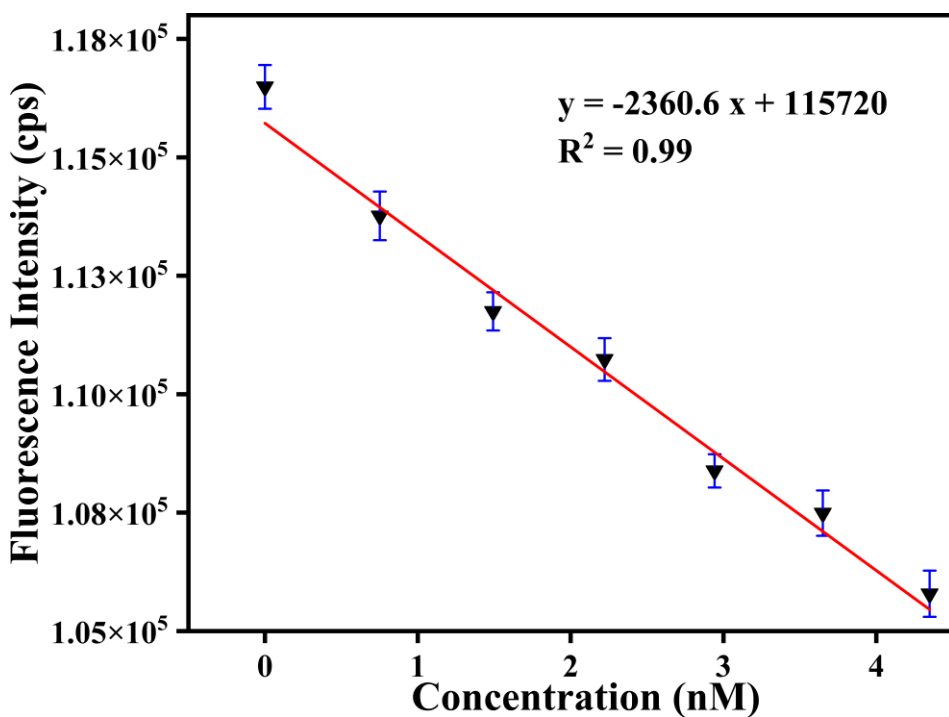
Figure S49. Change in the fluorescence intensity of **1'** in water as a function of concentration of furaltadone (FLT) (blue colour error bars signify the standard deviations of three individual measurements).
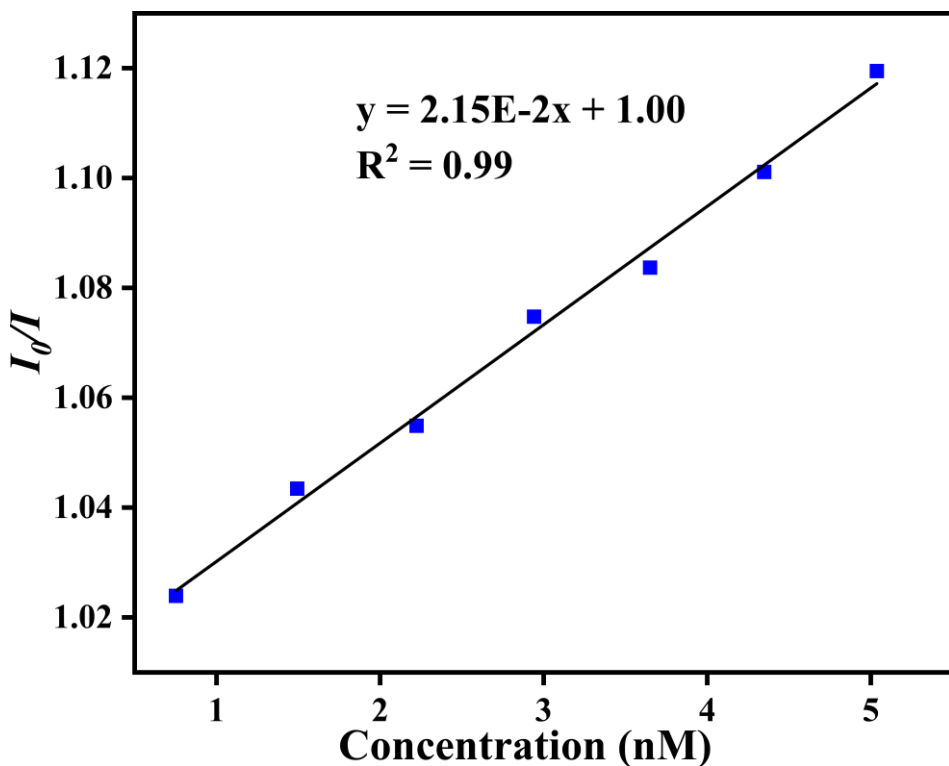
Figure S50. Stern-Volmer plot for the fluorescence quenching of **1'** in presence of furaltadone (FLT) in aqueous medium.
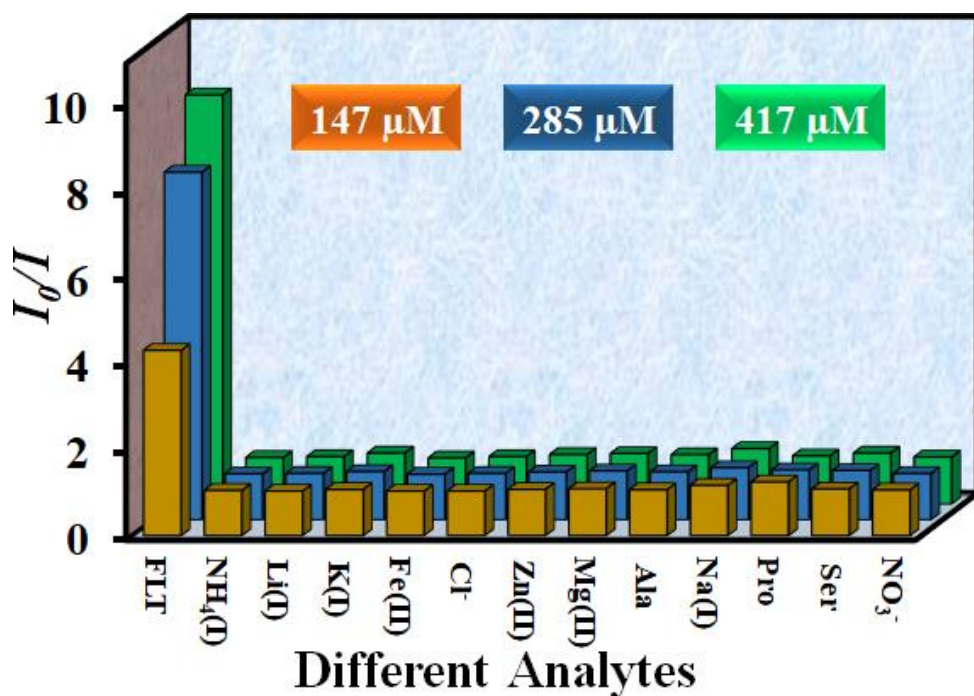
Figure S51. 3-D Stern-Volmer plots for furaltadone (FLT) sensing.
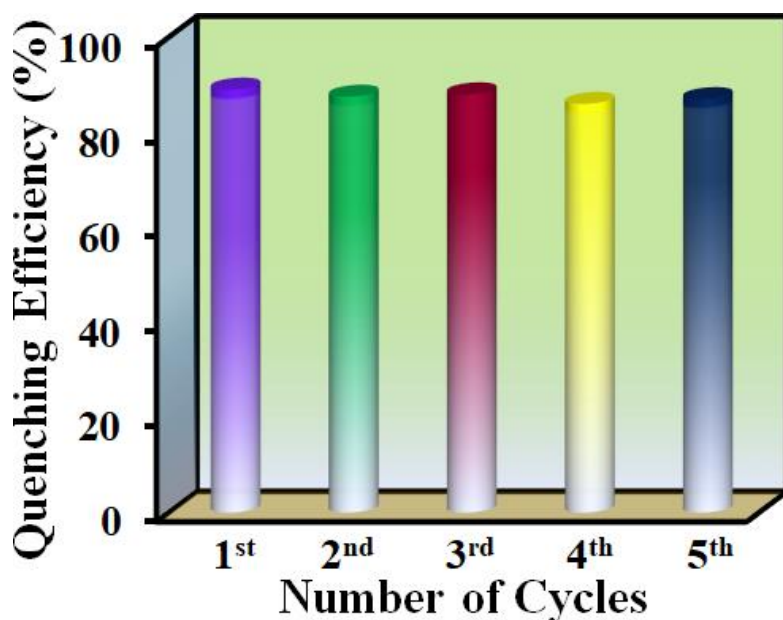
Figure S52. Reusability of the probe **1'** for furaltadone (FLT) sensing in aqueous medium.

Table S5. Fluorescence lifetimes of **1′** before and after the addition of furaltadone (FLT) solution (λ_{ex} = 375 nm, pulsed diode laser).

Volume of FLT Solution Added (μL)	α_1	τ_1 (ns)	$<\tau>*$ (ns)	χ^2
0	1	12.5	15.20	1.12
300	1	3.9	3.9	0.95

$<\tau>* = \alpha_1\tau_1$

Table S6. Evaluation of intra-day, inter-day accuracy and precision study of change in fluorescence intensity of **1′** after incremental addition of 5 mM aqueous solution of DNOC.

Type of Precision	Amount of FLT Added (µL)	Fluorescence Intensity			Average Intensity (cps)	SD	Error	RSD (%)
Intra Day	0	128845.5	129772.3	128809.9	129142.6	545.7	0.002	0.23
	50	56947.1	56489.1	56331.9	56589.4	319.6	-0.006	-0.63
	100	29964.7	29901.0	29720.8	29862.2	126.5	-0.003	-0.34
	150	16433.3	16230.6	16287.4	16317.1	104.6	-0.007	-0.71
	200	10243.7	10191.2	10187.1	10207.3	31.6	-0.004	-0.36
	250	7825.1	7783.0	7559.8	7722.6	142.6	-0.013	-1.31
	300	6244.2	6237.6	6050.2	6177.3	110.2	-0.011	-1.07
Inter Day	0	128809.9	129344.2	128721.8	128958.6	336.8	0.001	0.12
	50	56331.9	56536.3	56215.1	56361.1	162.6	0.001	0.05
	100	29720.8	29513.8	29471.7	29568.8	133.4	-0.005	-0.51
	150	16287.4	16232.5	16037.8	16185.9	131.2	-0.006	-0.62
	200	10187.1	10113.5	9963.4	10088.0	114.0	-0.010	-0.97
	250	7559.8	7667.5	7583.3	7603.5	56.6	0.006	0.58
	300	6050.2	6149.1	5946.3	6048.5	101.4	0.000	-0.03

Table S7. Comparison between the spiked and observed concentrations and recovery percentages of furaltadone (FLT) in serum and urine samples.

Type of Sample	Spiked Conc. of FLT (µM)	Observed Conc. of DNOC (µM)	Recovery (%)
Serum	11.9	12.2	102.5
	23.7	23.4	98.7
	35.1	35.3	100.5
Urine	11.9	11.8	99.1
	23.7	23.2	97.8
	35.1	34.9	98.9

Table S8. Comparison between the spiked and observed concentrations and recovery percentages of DNOC in different real water specimens.

Type of Water	Spiked Conc. of DNOC (μM)	Observed Conc. of DNOC (μM)	Recovery (%)
Milli-Q Water	11.9	11.6	97.5
	23.7	23.2	97.9
	35.1	35.2	100.3
Tap Water	11.9	12.1	102.5
	23.7	23.8	100.7
	35.1	34.9	99.5
Lake Water	11.9	11.6	97.6
	23.7	23.9	100.8
	35.1	35.3	100.6
River Water	11.9	12.2	102.5
	23.7	23.4	98.7
	35.1	34.9	99.4

Table S9. Comparison between the spiked and observed concentrations and recovery percentages of furaltadone (FLT) in different real water specimens.

Type of Water	Spiked Conc. of FLT (μM)	Observed Conc. of FLT (μM)	Recovery (%)
Milli-Q Water	11.9	12.1	102.0
	23.7	23.8	100.5
	35.1	34.9	99.5
Tap Water	11.9	11.6	97.6
	23.7	23.6	99.5
	35.1	35.2	100.4
Lake Water	11.9	11.7	98.2
	23.7	23.4	98.7
	35.1	35.3	100.6
River Water	11.9	11.6	97.3
	23.7	23.2	98.1
	35.1	35.2	100.4
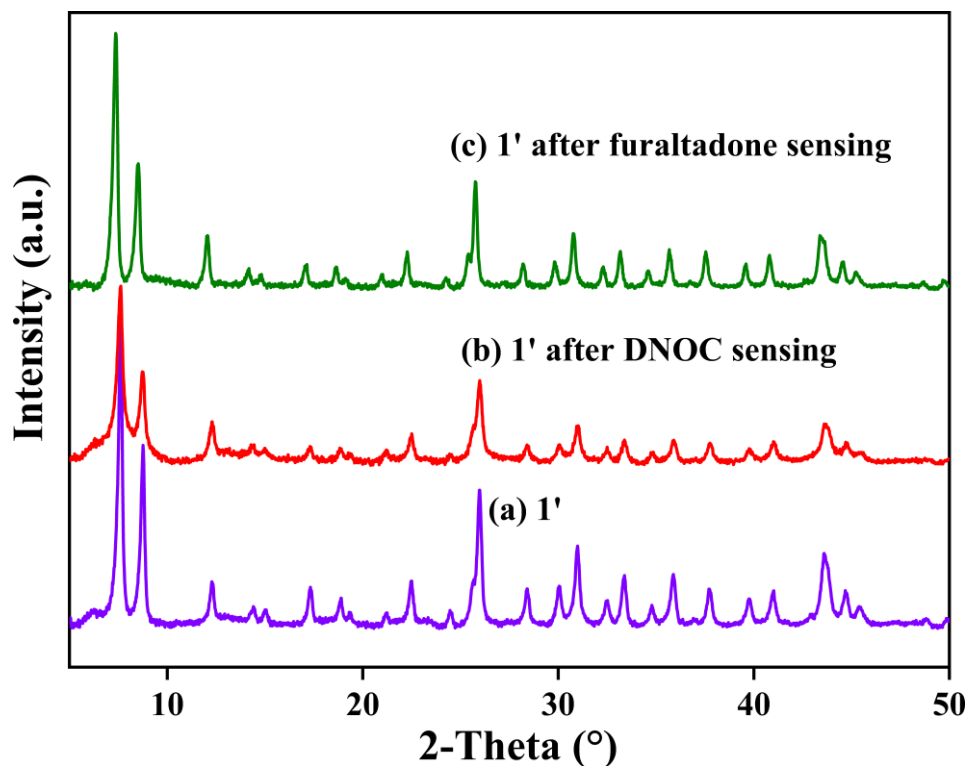
Figure S53. PXRD profiles of **1'** after DNOC and furaltadone (FLT) sensing.
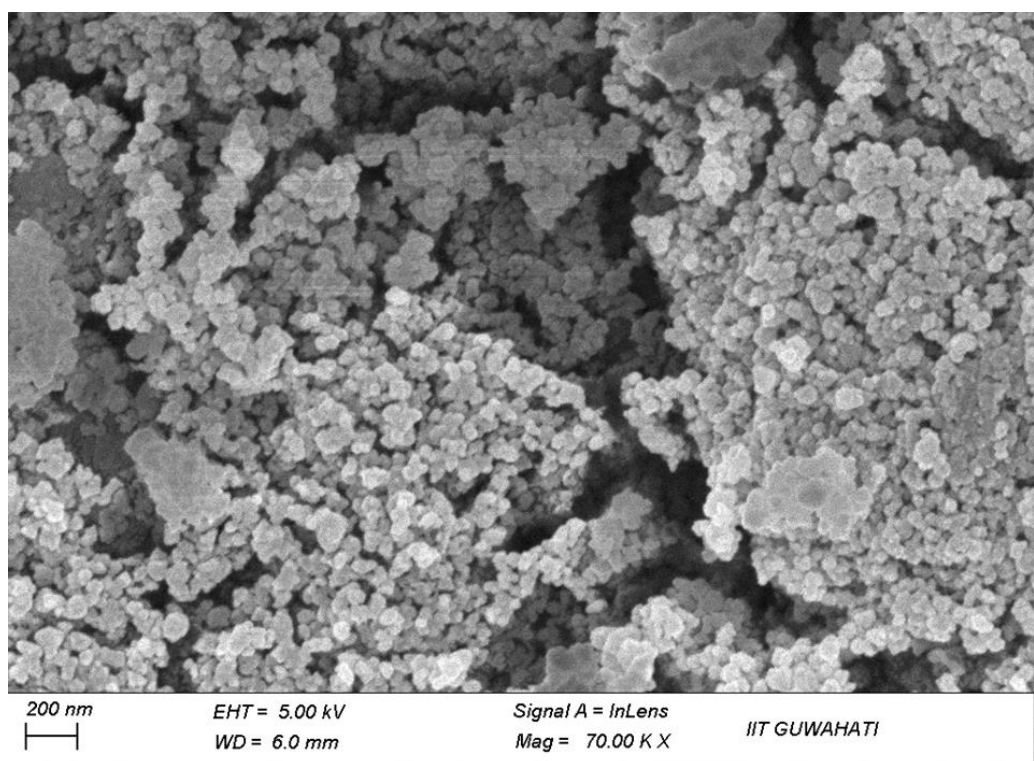
Figure S54. FE-SEM image of **1** after DNOC sensing.
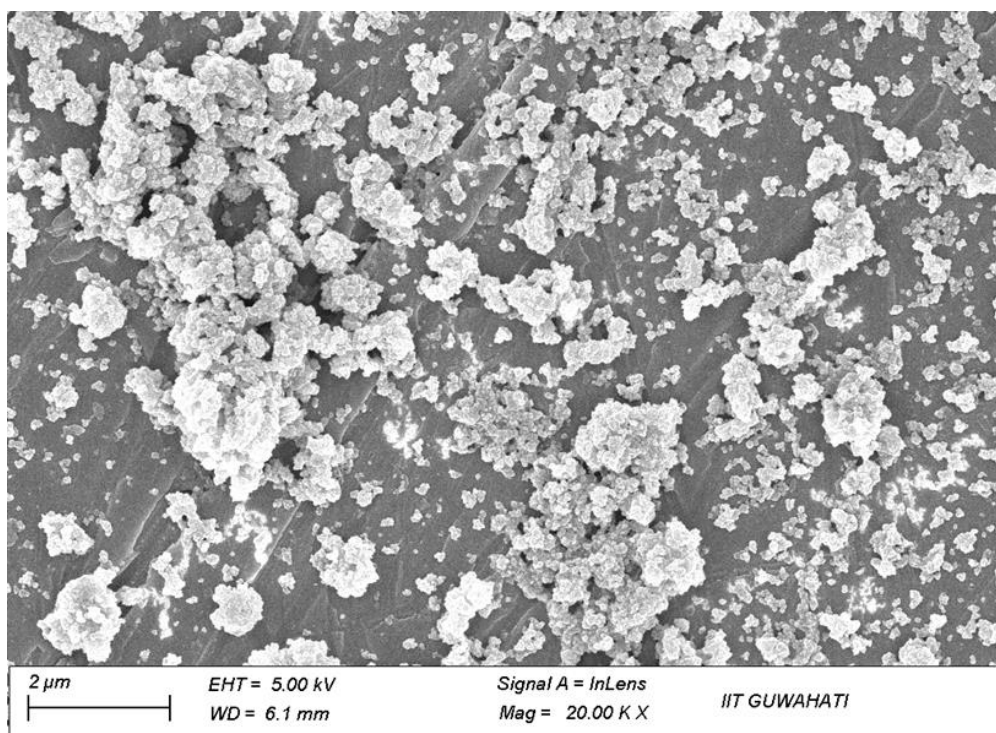
Figure S55. FE-SEM image of **1** after furaltadone (FLT) sensing.
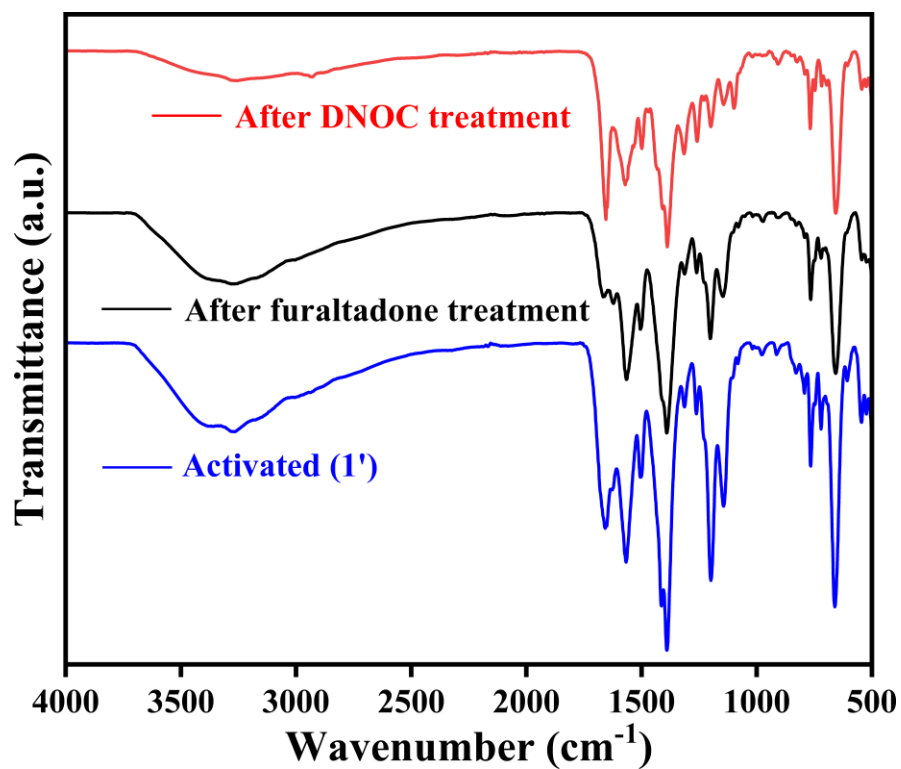
Figure S56. ATR-IR spectra of **1'** before and after treatment of DNOC and furaltadone (FLT).

Table S10. Comparison of the response time, detection limit and analyte used for the reported fluorescence based chemosensors of DNOC in the literature.

Sl. No.	Sensor Material	Type of Material	Sensing Medium	Mode of Detection	Detection Limit	Response Time	K_{sv} (M^{-1})	Ref.
1	**[Zr$_6$O$_4$(OH)$_4$(C$_{12}$H$_8$N$_4$O$_4$)$_4$(CF$_3$CO$_2$)$_2$] (1')**	MOF	water	turn-off	0.5 nM	5 s	$5 \cdot \times 10^7$	**this work**
2	Ethyleneglycol esters of 1-pyrene carboxylic acid	organic-molecules	H$_2$O : THF (99.9 : 0.1 (v/v))	turn-off	101 ppb and 223 ppb	-	$3.07 \cdot \times 10^4$ and 3.14×10^4	5
3	6,8-bis-(thiopen-2-yl)-1,3,7-triazapyrene	organic-molecule	tris buffer	turn-off	2397 ppb	-	$0.35 \cdot \times 10^4$	6

Table S11. Comparison of the response time, detection limit and analyte used for the reported fluorescence based chemosensors of furaltadone (FLT) in the literature.

Sl. No.	Sensor Material	Type of Material	Sensing Medium	Mode of Detection	Detection Limit	Response Time	K_{sv} (M^{-1})	Ref.
1	**[Zr$_6$O$_4$(OH)$_4$(C$_{12}$H$_8$N$_4$O$_4$)$_4$(CF$_3$CO$_2$)$_2$] (1')**	MOF	water	turn-off	1.1 nM	5 s	$2.1 \cdot \times 10^7$	**this work**
2	Tryptophan-capped gold nanoclusters	nano-clusters	buffer solution of pH 6.0	turn-off	0.087 μM	30s	-	7
3	Cu NCs@PVP	nano-clusters	PBS (pH = 6.0)	turn-off	0.045 μM	90 s	-	8
4	Histidine-Cu NCs	nano-clusters	PBS solution (pH = 8)	turn-off	0.085 μM	10 s	4.3×10^3	9
5	Cd$_3$(L1)(MTC)$_2$(H$_2$O)$_6$ L1 = (E)-4,4′-(ethene-l,2-diyl)bis(N-pyridin-3-yl)benzamide)	coordination polymers	water	turn-off	94 nM	-	2.2×10^5	10
6	[M(L)(HCPG)$_2$(H$_2$O)$_2$] (M = Co, Ni)	coordination polymers	water	turn-off	0.7 μM 0.22 μM	49 s 35 s	2.3×10^4 4.1×10^4	11

Details for structural modelling of Compound 1:

We used molecular mechanics to model the solvent-free structure of compound **1**, utilizing the universal force field (UFF) through the Forcite module in Biovia Materials Studio.[12] We began our homology modelling of the unknown structure of **1** with the reported MOF structure (MOR-2) as our reference point.[13]

Simulated Crystallographic Information File (CIF) for Guest-Free Compound 1.

data_Compound 1

_audit_creation_date   2024-09-04

_audit_creation_method   'Materials Studio'

_symmetry_space_group_name_H-M   'P-4'

_symmetry_Int_Tables_number   81

_symmetry_cell_setting   tetragonal

loop_

_symmetry_equiv_pos_as_xyz

 x,y,z

 -x,-y,z

 y,-x,-z

 -y,x,-z

_cell_length_a   14.6770

_cell_length_b   14.6770

_cell_length_c   20.7940

_cell_angle_alpha   90.0000

_cell_angle_beta   90.0000

_cell_angle_gamma   90.0000

loop_

_atom_site_label

_atom_site_type_symbol

_atom_site_fract_x

_atom_site_fract_y

_atom_site_fract_z

_atom_site_U_iso_or_equiv

_atom_site_adp_type

_atom_site_occupancy

O1	O	1.00304	0.11619	0.05899	0.00500	Uiso	1.00
O2	O	0.17109	0.16303	0.08801	0.08000	Uiso	1.00
O3	O	0.08985	0.08885	0.16728	0.08000	Uiso	1.00
C4	C	0.15209	0.14683	0.14840	0.08000	Uiso	1.00
C5	C	0.20513	0.19867	0.20022	0.08000	Uiso	1.00
C6	C	0.16474	0.21513	0.26102	0.08000	Uiso	1.00
C7	C	0.29496	0.23377	0.19082	0.08000	Uiso	1.00
N8	N	0.34693	0.21232	0.13440	0.10000	Uiso	0.50
O9	O	0.49816	0.61626	0.55897	0.00500	Uiso	1.00
O10	O	0.66241	0.67074	0.58759	0.08000	Uiso	1.00
O11	O	0.58582	0.59276	0.66713	0.08000	Uiso	1.00
C12	C	0.64427	0.65434	0.64794	0.08000	Uiso	1.00
C13	C	0.69559	0.70886	0.69914	0.08000	Uiso	1.00
C14	C	0.68288	0.68960	0.76512	0.08000	Uiso	1.00
C15	C	0.75964	0.77867	0.68409	0.08000	Uiso	1.00
N16	N	0.77478	0.80653	0.61904	0.10000	Uiso	0.50
O17	O	0.88401	1.00296	0.05860	0.00500	Uiso	1.00
O18	O	0.83763	0.17074	0.08863	0.08000	Uiso	1.00
O19	O	0.91509	0.09180	0.16753	0.08000	Uiso	1.00
C20	C	0.85623	0.15300	0.14893	0.08000	Uiso	1.00
C21	C	0.80562	0.20532	0.20112	0.08000	Uiso	1.00
C22	C	0.82508	0.19196	0.26669	0.08000	Uiso	1.00
C23	C	0.73713	0.26890	0.18656	0.08000	Uiso	1.00
O24	O	0.38416	0.49803	0.55880	0.00500	Uiso	1.00
O25	O	0.33449	0.66772	0.58823	0.08000	Uiso	1.00
O26	O	0.41163	0.58913	0.66735	0.08000	Uiso	1.00
C27	C	0.35284	0.65028	0.64840	0.08000	Uiso	1.00

C28	C	0.30095	0.70194	0.69997	0.08000	Uiso	1.00
C29	C	0.28524	0.66157	0.76008	0.08000	Uiso	1.00
C30	C	0.26491	0.78979	0.69017	0.08000	Uiso	1.00
O31	O	0.25284	0.07150	-0.00471	0.08000	Uiso	0.50
O32	O	0.08569	0.24887	0.00557	0.08000	Uiso	0.50
Zr33	Zr	0.11610	0.11020	-0.00006	0.00500	Uiso	1.00
C34	C	0.70986	1.00807	-0.00770	0.00000	Uiso	1.00
O35	O	0.74993	0.58435	0.49748	0.08000	Uiso	0.50
O36	O	0.57280	0.75256	0.50232	0.08000	Uiso	0.50
Zr37	Zr	0.61109	0.61499	0.49984	0.00500	Uiso	1.00
C38	C	0.20915	0.49348	0.49632	0.00000	Uiso	1.00
C39	C	0.10927	0.49266	0.49488	0.00000	Uiso	1.00
C40	C	0.61053	0.00931	-0.01118	0.00000	Uiso	1.00
H41	H	0.09670	0.19019	0.27084	0.00000	Uiso	1.00
H42	H	0.33467	0.15167	0.10962	0.00000	Uiso	1.00
N43	N	0.42215	0.26666	0.11779	0.00000	Uiso	1.00
H44	H	0.63550	0.63705	0.77983	0.00000	Uiso	1.00
H45	H	0.72021	0.83630	0.59464	0.00000	Uiso	1.00
N46	N	0.86332	0.82360	0.59668	0.00000	Uiso	1.00
H47	H	0.87824	0.14449	0.28022	0.00000	Uiso	1.00
H48	H	0.72001	0.28095	0.13734	0.00000	Uiso	1.00
H49	H	0.31000	0.59292	0.76769	0.00000	Uiso	1.00
H50	H	0.27674	0.82432	0.64499	0.00000	Uiso	1.00
F51	F	0.07873	0.53324	0.55076	0.00000	Uiso	1.00
F52	F	0.07708	0.40409	0.49130	0.00000	Uiso	1.00
F53	F	0.08051	0.54155	0.44178	0.00000	Uiso	1.00
F54	F	0.57945	-0.01933	0.04791	0.00000	Uiso	1.00
F55	F	0.58253	-0.04945	-0.05924	0.00000	Uiso	1.00
F56	F	0.57948	0.09625	-0.02424	0.00000	Uiso	1.00
C57	C	0.07266	0.23704	0.60034	0.00000	Uiso	1.00

C58   C   0.76207 0.48626 0.91971 0.00000 Uiso 1.00

C59   C   1.01944 0.78578 0.57875 0.00000 Uiso 1.00

H60   H   0.91256 0.69470 0.61725 0.00000 Uiso 1.00

C61   C   0.29792 0.43813 0.93719 0.00000 Uiso 1.00

N62   N   0.27642 1.08020 0.44204 0.00000 Uiso 1.00

C63   C   0.22613 1.15364 0.45811 0.00000 Uiso 1.00

C64   C   0.13561 1.13652 0.44628 0.00000 Uiso 1.00

N65   N   0.12864 1.05174 0.42319 0.00000 Uiso 1.00

H66   H   0.48435 0.16974 0.06125 0.00000 Uiso 1.00

N67   N   0.63266 0.26998 0.02652 0.00000 Uiso 1.00

C68   C   0.68747 0.34340 0.02379 0.00000 Uiso 1.00

C69   C   0.64896 0.41409 0.05789 0.00000 Uiso 1.00

N70   N   0.56964 0.38505 0.08241 0.00000 Uiso 1.00

H71   H   0.75362 0.34345 0.00113 0.00000 Uiso 1.00

H72   H   0.67793 0.48090 0.06592 0.00000 Uiso 1.00

H73   H   0.74662 0.78433 0.47813 0.00000 Uiso 1.00

H74   H   0.92098 0.81745 0.45371 0.00000 Uiso 1.00

H75   H   0.67095 0.50262 0.58614 0.00000 Uiso 1.00

H76   H   0.57833 0.52500 0.88830 0.00000 Uiso 1.00

H77   H   0.98146 0.06988 0.59160 0.00000 Uiso 1.00

H78   H   0.82839 1.00428 0.08540 0.00000 Uiso 1.00

Zr79 Zr   0.00000 0.00000 0.11528 0.00500 Uiso 1.00

Zr80 Zr   0.50000 0.50000 0.61534 0.00500 Uiso 1.00

loop_

_geom_bond_atom_site_label_1

_geom_bond_atom_site_label_2

_geom_bond_distance

_geom_bond_site_symmetry_2

_ccdc_geom_bond_type

O1   Zr33   2.065   4_655 S

O1	Zr33	2.066	1_655	S
O1	Zr79	2.069	1_655	S
O2	C4	1.308	.	A
O2	Zr33	2.146	.	S
O3	C4	1.309	.	A
O3	Zr79	2.147	.	S
C4	C5	1.532	.	S
C5	C6	1.417	.	A
C5	C7	1.429	.	A
C6	C30	1.417	4_656	A
C6	H41	1.083	.	S
C7	N8	1.434	.	S
C7	C29	1.421	4_656	A
N8	H42	1.044	.	S
N8	N43	1.405	.	S
O9	Zr37	2.064	.	S
O9	Zr80	2.070	.	S
O9	Zr37	2.064	4_656	S
O10	C12	1.305	.	A
O10	Zr37	2.137	.	S
O11	C12	1.308	.	A
O11	Zr80	2.145	.	S
C12	C13	1.530	.	S
C13	C14	1.413	.	A
C13	C15	1.425	.	A
C14	C23	1.413	4_656	A
C14	H44	1.083	.	S
C15	N16	1.430	.	S
C15	C22	1.420	4_656	A
N16	H45	1.044	.	S

N16	N46	1.403	.	S
O17	Zr33	2.061	2_665	S
O17	Zr79	2.071	1_665	S
O17	Zr33	2.061	4_665	S
O17	H78	0.989	.	S
O18	C20	1.310	.	A
O18	Zr33	2.150	4_655	S
O19	C20	1.305	.	A
O19	Zr79	2.133	1_655	S
C20	C21	1.523	.	S
C21	C22	1.407	.	A
C21	C23	1.405	.	A
C22	C15	1.420	3_566	A
C22	H47	1.083	.	S
C23	C14	1.413	3_566	A
C23	H48	1.069	.	S
O24	Zr37	2.059	4_656	S
O24	Zr80	2.067	.	S
O24	Zr37	2.064	2_665	S
O24	H75	0.989	2_665	S
O25	C27	1.305	.	A
O25	Zr37	2.143	4_656	S
O26	C27	1.306	.	A
O26	Zr80	2.136	.	S
C27	C28	1.518	.	S
C28	C29	1.402	.	A
C28	C30	1.408	.	A
C29	C7	1.421	3_566	A
C29	H49	1.083	.	S
C30	C6	1.417	3_566	A

C30	H50	1.082	.	S
O31	Zr33	2.088	.	S
O31	C34	1.291	2_665	A
O32	Zr33	2.087	.	S
O32	C34	1.291	3_465	A
Zr33	O17	2.061	2_665	S
Zr33	O18	2.150	3_565	S
Zr33	O1	2.065	3_565	S
Zr33	O1	2.066	1_455	S
Zr33	O17	2.061	3_465	S
C34	O31	1.291	2_665	A
C34	C40	1.460	1_565	S
C34	O32	1.291	4_665	A
O35	Zr37	2.087	.	S
O35	C38	1.291	2_665	A
O36	Zr37	2.097	.	S
O36	C38	1.293	3_566	A
Zr37	O25	2.143	3_566	S
Zr37	O24	2.059	3_566	S
Zr37	O24	2.064	2_665	S
Zr37	O9	2.064	3_566	S
C38	C39	1.466	.	S
C38	O35	1.291	2_665	A
C38	O36	1.293	4_656	A
C39	F51	1.381	.	S
C39	F52	1.385	.	S
C39	F53	1.383	.	S
C40	C34	1.460	1_545	S
C40	F54	1.376	.	S
C40	F55	1.383	.	S

C40	F56	1.382	.	S
N43	C58	1.293	3_566	D
N46	C57	1.297	2_665	D
C57	N46	1.297	2_665	D
C57	C59	1.463	2_665	S
C57	H60	1.084	2_665	S
C58	N43	1.293	4_656	D
C58	C61	1.462	2_665	S
C58	H66	1.077	4_656	S
C59	C57	1.463	2_665	S
C59	N62	1.347	3_566	D
C59	N65	1.343	3_566	S
H60	C57	1.084	2_665	S
C61	C58	1.462	2_665	S
C61	N67	1.348	3_566	D
C61	N70	1.347	3_566	S
N62	C63	1.348	.	S
N62	C59	1.347	4_656	D
C63	C64	1.374	.	D
C63	H73	1.078	2_675	S
C64	N65	1.338	.	S
C64	H74	1.082	2_675	S
N65	C59	1.343	4_656	S
N65	H77	1.037	3_576	S
H66	C58	1.077	3_566	S
N67	C68	1.346	.	S
N67	C61	1.348	4_656	D
C68	C69	1.378	.	D
C68	H71	1.079	.	S
C69	N70	1.341	.	S

C69	H72	1.082	.	S
N70	C61	1.347	4_656	S
N70	H76	1.044	3_566	S
H73	C63	1.078	2_675	S
H74	C64	1.082	2_675	S
H75	O24	0.989	2_665	S
H76	N70	1.044	4_656	S
H77	N65	1.037	4_756	S
Zr79	O3	2.147	2	S
Zr79	O17	2.071	2_665	S
Zr79	O17	2.071	1_445	S
Zr79	O1	2.069	1_455	S
Zr79	O1	2.069	2_655	S
Zr79	O19	2.133	1_455	S
Zr79	O19	2.133	2_655	S
Zr80	O11	2.145	2_665	S
Zr80	O26	2.136	2_665	S
Zr80	O9	2.070	2_665	S
Zr80	O24	2.067	2_665	S

References:

1. O. K. Farha, A. Özgür Yazaydın, I. Eryazici, C. D. Malliakas, B. G. Hauser, M. G. Kanatzidis, S. T. Nguyen, R. Q. Snurr and J. T. Hupp, *Nat. Chem.*, 2010, **2**, 944-948.
2. C. A. Parker and W. Rees, *Analyst*, 1960, **85**, 587-600.
3. S. Nandi, E. Sharma, V. Trivedi and S. Biswas, *Inorg. Chem.*, 2018, **57**, 15149-15157.
4. J. H. Cavka, S. Jakobsen, U. Olsbye, N. Guillou, C. Lamberti, S. Bordiga and K. P. Lillerud, *J. Am. Chem. Soc.*, 2008, **130**, 13850-13851.
5. I. Kovalev, L. Sadieva, O. Taniya, D. Kopchuk, G. Zyryanov, E. Ulomsky, V. Rusinov and O. Chupakhin, *Chimica Techno Acta.*, 2021, **8**.
6. I. A. Lavrinchenko, T. D. Moseev, M. V. Varaksin, G. V. Zyryanov, O. S. Taniya, A. N. Tsmokalyuk, O. P. Demidov, I. V. Borovlev, V. N. Charushin and O. N. Chupakhin, *New J Chem.*, 2022, **46**, 5121-5128.

7. Z. Cai, H. Li, X. Yang, M. Zhang, J. Guo, Y. Su and T. Liu, *Spectrochim. Acta A Mol. Biomol. Spectrosc.*, 2024, **308**, 123748.

8. Z.-f. Cai, X.-s. Wang, H.-y. Li, P.-l. Cao, X.-r. Han, P.-y. Guo, F.-y. Cao, J.-x. Liu, X.-x. Sun and T. Li, *Spectrochim. Acta A Mol. Biomol. Spectrosc.*, 2022, **279**, 121408.

9. S. Zhang, M.-l. Jin, Y.-x. Gao, W.-q. Li, X.-y. Wang, X.-x. Li, J.-q. Qiao and Y. Peng, *Chem. Pap.*, 2022, **76**, 7855-7863.

10. J. Geng, J. Sun, H. Lin and X. Wang, *New J. Chem.*, 2023, **47**, 9701-9707.

11. J. Geng, Y. Chen, S. Xie, H. Lin and X. Wang, *Inorg. Chem.*, 2023, **62**, 5158-5167.

12. A. K. Rappé, C. J. Casewit, K. Colwell, W. A. Goddard III and W. M. Skiff, *J. Am. Chem. Soc.*, 1992, **114**, 10024-10035.

13. S. Rapti, D. Sarma, S. A. Diamantis, E. Skliri, G. S. Armatas, A. C. Tsipis, Y. S. Hassan, M. Alkordi, C. D. Malliakas and M. G. Kanatzidis, *J. Mater. Chem. A*, 2017, **5**, 14707-14719.